Science of the Total Environment 858 (2023) 159315

Contents lists available at ScienceDirect

Science of the Total Environment

journal homepage: www.elsevier.com/locate/scitotenv

Characteristics of fine and ultrafine aerosols in the London underground

Prashant Kumar [a,b,c,*], Juan C. Zavala-Reyes [a,g], Gopinath Kalaiarasan [a], Hisham Abubakar-Waziri [d], Gloria Young [e], Ian Mudway [f], Claire Dilliway [h], Ramzi Lakhdar [d], Sharon Mumby [d], Michał M. Kłosowski [e], Christopher C. Pain [h], Ian M. Adcock [d], Jonathan S. Watson [h], Mark A. Sephton [h], Kian Fan Chung [d], Alexandra E. Porter [e]

[a] Global Centre for Clean Air Research (GCARE), School of Sustainability, Civil and Environmental Engineering, Faculty of Engineering and Physical Sciences, University of Surrey, Guildford GU2 7XH, Surrey, UK
[b] Department of Civil, Structural & Environmental Engineering, Trinity College Dublin, Dublin, Ireland
[c] School of Architecture, Southeast University, Nanjing, China
[d] National Heart & Lung Institute, Imperial College London, London, UK
[e] Department of Materials, Imperial College London, London, UK
[f] National Institute of Health Research, Health Protection Research Unit in Environmental Exposures and Health, Imperial College London, London, UK
[g] Escuela Nacional de Estudios Superiores, Unidad Mérida, UNAM, Carretera Mérida-Tetiz, Km 4.5, Ucú, Yucatán, 97357, Mexico
[h] Department of Earth Science and Engineering, Imperial College London, UK

HIGHLIGHTS

- 70 % (N-OpHrs) and 64 % (OpHrs) of the PNCs were found in nucleation mode.
- Low fresh air exchange (0.24 ± 0.11 times/h) indicates need for better ventilation.
- PM peaks correlated (r_{pb} > 0.40) well with train arrival times at the platform.
- RDD was higher for $PM_{2.5–10}$ and PNCs in nucleation mode than their counterparts.
- $PM_{0.1–1}/PM_{0.1}$ contained magnetite (<20 nm) and redox-active metal traces (Cr, Ni, Mn).

GRAPHICAL ABSTRACT

ARTICLE INFO

Guest Editor: Fang Wang

Keywords:
Underground pollution
Exposure assessment
Particle characterisation
Subway station
Metal content

ABSTRACT

Underground railway systems are recognised spaces of increased personal pollution exposure. We studied the number-size distribution and physico-chemical characteristics of ultrafine ($PM_{0.1}$), fine ($PM_{0.1–2.5}$) and coarse ($PM_{2.5–10}$) particles collected on a London underground platform. Particle number concentrations gradually increased throughout the day, with a maximum concentration between 18:00 h and 21:00 h (local time). There was a maximum decrease in mass for the $PM_{2.5}$, $PM_{2.5–10}$ and black carbon of 3.9, 4.5 and ~ 21-times, respectively, between operable (OpHrs) and non-operable (N-OpHrs) hours. Average PM_{10} (52 μg m^{-3}) and $PM_{2.5}$ (34 μg m^{-3}) concentrations over the full data showed levels above the World Health Organization Air Quality Guidelines. Respiratory deposition doses of particle number and mass concentrations were calculated and found to be two- and four-times higher during OpHrs compared with N-OpHrs, reflecting events such as train arrival/departure during OpHrs. Organic compounds were composed of aromatic hydrocarbons and polycyclic aromatic hydrocarbons (PAHs) which are known to be harmful to health. Specific ratios of PAHs were identified for underground transport that may reflect an interaction between PAHs and fine particles. Scanning transmission electron microscopy (STEM) chemical maps of fine and ultrafine fractions show they are composed of Fe and O in the form of magnetite and nanosized mixtures of metals including Cr, Al,

* Corresponding author at: Global Centre for Clean Air Research (GCARE), School of Sustainability, Civil and Environmental Engineering, Faculty of Engineering and Physical Sciences, University of Surrey, Guildford GU2 7XH, Surrey, UK.
E-mail addresses: P.Kumar@surrey.ac.uk Prashant.Kumar@cantab.net (P. Kumar).

http://dx.doi.org/10.1016/j.scitotenv.2022.159315
Received 24 June 2022; Received in revised form 15 September 2022; Accepted 5 October 2022
Available online 22 October 2022

Ni and Mn. These findings, and the low air change rate (0.17 to 0.46 h^{-1}), highlight the need to improve the ventilation conditions.

Abbreviations

ACH	Air change rate
BC	Black carbon
CO	carbon monoxide
CO_2	Carbon dioxide
EDXS	Energy dispersive x-ray spectroscopy
ESEM	Environmental scanning electron microscopy
FEG	Field emission gun
GC–MS	Gas chromatography-mass spectrometry
ICP-MS	Inductively coupled plasma mass spectrometry
N-OpHrs	Non-operable hours
NP	Nanoparticle
OpHrs	Operable hours
PAH	Polycyclic aromatic hydrocarbon
PM	Particulate matter
PNC	Particle number concentration
PND	Particle number distribution
PTFE	Poly tetra fluoro ethylene (Teflon)
PUF	Polyurethane foams
RDD	Respiratory deposition dose
SEM	Scanning electron microscopy
TEM	Transmission electron microscopy
STEM	Scanning transmission electron microscopy
UFP	Ultrafine particles
XRD	X-ray diffraction

1. Introduction

Urban planners seek to decrease pollution levels in urban areas by incentivising the use of alternative modes of public transport, including underground or metro systems with electric trains. These rail systems reduce traffic congestion and dependence on private vehicles and potentially improve urban air quality (Yang et al., 2018). Around 2.8 million trips are taken each day on the London Underground, with an estimated mean journey time of 47 min (Smith et al., 2020; TfL, 2020). Parts of the London underground are over 150 years old; the rest of the Underground system continues to develop rapidly. With similar patterns of development in other cities around the world, the confined underground environment and poor ventilation system raises concerns regarding elevated particle concentrations (Mendes et al., 2018). As subway systems develop and grow worldwide, human exposure to air pollutants in underground environments and related health risks such as heart disease, stroke, lung cancer, and respiratory disorders, have become a significant public concern (Smith et al., 2020; Loxham and Nieuwenhuijsen, 2019; Grana et al., 2017; Chen et al., 2021).

Investigations have found the airborne particulate matter (PM) load to be significantly higher in underground metro systems than the outdoor ambient air (Cartenì et al., 2020; Smith et al., 2020; Mohsen et al., 2018; Perrino et al., 2015; Rivas et al., 2017a, 2017b; Wang and Oliver Gao, 2011). A summary of relevant literature on the average concentration levels of fine (≤ 2.5 μm in aerodynamic diameter; $PM_{2.5}$) and ultrafine (≤ 0.1 μm; $PM_{0.1}$ or UFP) particles for different underground stations in London and cities around the world is presented in Table 1. PM levels in the London underground system are much higher than in roadside environments (COMEAP, 2018), with concentrations in the range of 270–480 μg m^{-3} (Seaton et al., 2005).

Other work has reported concentrations of $PM_{2.5}$ mass in underground environments 4-times higher than in outdoor background locations, e.g. 88 μg m^{-3} in the London underground compared with 19 and 22 μg m^{-3} at ambient background locations and roadside environments in central London, respectively (Smith et al., 2020). These higher levels of particle concentrations in London Underground stations are primarily influenced by ventilation settings, depth and age of the tunnels, and are highest in the deepest underground lines (Smith et al., 2020). However, there is little data available on the air pollution exposure profiles of London Underground commuters (Rivas et al., 2017a, 2017b). Furthermore, prior studies have not measured continuous variations of fine and ultrafine particles for a longer period of time.

The sources and aerodynamic diameter of underground pollution are very different to roadside environments. PM sources in the underground are largely from non-exhaust emissions, resulting from high train braking frequency leading to brake pad wear as well as the wear of train components such as wheels, brake blocks, collector shoes and stick lubes (Minguillón et al., 2018; Harrison et al., 2012). Other sources, including the wear of rails, grinding of rails, escalators and refurbishment work (Smith et al., 2020), are common to all underground stations around the world, where particles are resuspended by train movements that elevate PM concentrations (Querol et al., 2012). In general, the outdoor non-exhaust sources emit coarse particles with a diameter between 2.5 and 10 μm ($PM_{2.5–10}$). Sanders et al. (2003) undertook an investigation testing different brake pads to measure the PM mass concentrations generated and found that PM_{10} accounted for 63–85 % of the total brake wear mass, depending on the type of brake pad used. Wahlström et al. (2010) showed the characteristics of particle number distributions have higher peaks at 100 to 500 nm size range, independent of brake-pad type. The concentrations of London Underground PM with different aerodynamic diameters are expected to vary. No prior studies have measured the size-resolved distributions of all PM fractions, including the ultrafine fraction, on the London Underground or used these measurements to predict deposition profiles in the lung. This knowledge is important as it will significantly help to improve predictions of the toxicity and impact of Underground pollution on respiratory health.

Several studies have studied and characterised the phase chemistry and metal composition of unfractionated $PM_{2.5}$ or PM_{10} in underground train environments, including the London Underground (Martins et al., 2021; Smith et al., 2020; Mugica-Álvarez et al., 2012; Cheng et al., 2012; Kam et al., 2011b). On the London underground, the greatest fraction of $PM_{2.5}$, was made up of iron oxide (Fe_2O_3), with small contributions of quartz, traces of other metals in addition to 7 % elemental carbon, 11 % organic carbon, and 14 % metallic and mineral oxides (Smith et al., 2020; Seaton et al., 2005). Karlsson et al. (2005) showed that the majority of underground iron-rich PM was Magnetite (Fe_3O_4). One study on a busy railway station at the major terminal of an airport in Europe measured the presence of Fe, Cu, Zn, Mn and Cr metals in PM with a diameter of >180 nm (Loxham et al., 2013). Electron microscopic characterisation of the morphology and composition of fine and ultrafine PM collected on the Barcelona subway system has been reported (Moreno et al., 2015b). The fine and ultrafine PM was principally composed of ultrafine Fe oxides (mixtures of Magnetite, Hematite nanocrystals - probably the result of continued oxidation) generated by frictional wear. However, there has been no information detailing the composition and structure of UFP on the London Underground, which is one of the most polluted urban underground transport systems (Smith et al., 2020). It is important to address this knowledge gap as specific transition metals in the fine and ultrafine fractions generated from brake wear could cause oxidative damage and genotoxicity (Loxham et al., 2013; Bhabra et al., 2009; Charrier and Anastasio, 2015).

The aim of this work is to quantify the size-resolved distributions of aerosols from ultrafine to coarse size range in an underground environment, namely South Kensington tube station, a deep London underground railway system. In addition, we aim to provide an improved understanding

Table 1
Summary of relevant research studies reporting $PM_{2.5}$ and PNCs in underground environments.

Study location (country)	PM type	Average concentration of PM ($\mu g\ m^{-3}$) and PNC ($\#\ cm^{-3}$)	Description	Reference
Singapore (Singapore)	PM_{10} $PM_{2.5}$	~5–70 ~5–60	The study findings suggest that any ventilation improvements and station design must be focused on $PM_{2.5}$ exposure reduction.	Tan et al. (2022)
Stockholm (Sweden)	PM_{10} $PM_{2.5}$ PM_1	204 ± 180 102 ± 105 35 ± 34	Train frequency effect is more significant for PM_{10}, and the ventilation system notably decreases PM concentration at platform level.	Tu and Olofsson (2021)
Porto Alegre (Brazil)	$PM_{0.01–0.42}$	6.66×10^4	First study to measure the nanoparticles (NPs) and black carbon (BC) on two ground-level platforms in Brazil, showing predominance of NPs enriched with metals that increase oxidative stress like Cd, Fe, Pb, Cr, Zn, Ni, V, Hg, Sn, and Ba both on the platforms and inside train.	Lima et al. (2021)
Lisbon (Portugal)	$PM_{2.5}$	38 ± 21	$PM_{2.5}$ concentrations were found to be moderate compared to other city metros. The chemical composition analysis shows that the Fe element was found to be abundant in the metro PM sourced from rail-wheel-brake abrasions.	Martins et al. (2021)
London (UK)	$PM_{2.5}$	88	$PM_{2.5}$ concentrations in the London underground are many times higher than in other London transport environments. Failure to include this microenvironment will lead to misclassification in epidemiological studies.	Smith et al. (2020)
Beijing (China)	$PM_{2.5}$	165 ± 12	The analysis portrayed the average mass ratio of PM concentrations inside subway stations is about 68.7 %, much lower than outdoor conditions (79.6 %).	Pan et al. (2019)
Athens (Greece)	UFP (14.6–430 nm)	1.2×10^4	UFP concentrations showed a weak correlation with train passage frequency, and strong correlation with urban background particle concentrations. The size distribution was strongly influenced by outdoor conditions, such as the morning traffic rush hour and new particle formation events observed at noon.	Mendes et al. (2018)
Rome (Italy)	UFP	1.4×10^3	The concentrations of UFPs in underground train environments were found to be less and comparable to urban background levels. However, in underground trains the PM_{10} concentration values are much higher.	Grana et al. (2017)
Barcelona (Spain) Athens (Greece) Oporto (Portugal)	$PM_{2.5}$ $PM_{2.5}$ $PM_{2.5}$	58.3 ± 13.7 68.3 ± 11.3 83.7 ± 45.7	PM concentrations in all subway systems of these cities displayed clear diurnal patterns, depending largely on the operation and frequency of the trains and the ventilation system. PM concentrations inside the trains were greatly affected by the surrounding (i.e. platforms and tunnels) air quality conditions.	Martins et al. (2016)
Shanghai (China)	$PM_{2.5}$	177.7 ± 26.05	$PM_{2.5}$ concentrations were found to be higher. Also, the elements such as Fe, Mn, Cr, Cu, Sr, Ba and Pb concentrations are higher in the underground ambience compared to the urban air, implicating the association of these elements with the metro working process.	Guo et al. (2014)
New York (USA)	$PM_{2.5}$	100.1 ± 41.0	PM and BC soot levels in NYC's subways are considerably higher than ambient urban street levels and warrant further monitoring and investigation of BC and PM demonstrate similar results for subway exposures.	Vilcassim et al. (2014)
Mexico city (Mexico)	$PM_{2.5}$	60	The subway systems metals' concentrations were greater than the outdoors, exhibiting the presence of many individual particles with a large metal content in the subway samples.	Mugica-Álvarez et al. (2012)
Barcelona (Spain)	PM_{10} and $PM_{2.5}$	339 ± 46 and 115 ± 16	PM levels inside the trains in summer are found to be low compared to the PM levels on the platforms. The daily PM values were found to increase from 06:00 to 07 00 a.m., and from 07:00 to 10:00 p.m. But a marked decrease between 10:00 p.m. and 05:00 a.m.	Querol et al. (2012)
Los Angeles (USA)	PM_{10} and $PM_{2.5}$	78 and 57	The subway line commuters are greatly exposed to higher PM concentrations. Regression analysis showed that the subway line is less influenced by ambient PM levels. Strong correlations of $PM_{2.5}$ and PM_{10} found between train and stations reveal that PM from stations is the main source of PM inside trains.	Kam et al. (2011a)
Shanghai (China)	$PM_{2.5}$	287 ± 177	The study shows that fine particles or ultrafine particles constituted the preponderant fraction of metro station particulate matter.	Ye et al. (2010)
Paris (France)	PM_{10} and $PM_{2.5}$	329 ± 107 and 93 ± 34	The average daytime PM_{10} and $PM_{2.5}$ concentrations are approximately 5–30 times higher than those measured in Paris air quality monitoring site but lower than those measured in previous campaigns in subway systems.	Raut et al. (2009)

of the aerosols' physico-chemical composition, and uniquely of the ultrafine fraction, and likely exposure doses to the travelling public. The South Kensington tube station can be considered a worst-case scenario of exposure given that it is one of the deepest and oldest underground train systems in the world, in contrast to a well-ventilated overground platform where the pollution will be made up of a mixture of PM from overground and underground sources.

2. Materials and methods

We simultaneously monitored the airborne concentrations of PM_{10}, $PM_{2.5}$, PM_1 and the particle number concentrations (PNC) and distributions (PND) in the 6–10,000 nm size range (Section 2.2) while sampling PM mass in different size fractions (Section 2.3) on the underground platform of South Kensington station over a continuous duration of 23 days from 29 September to 22 October 2020 (Supplementary Information Fig. S1). carbon dioxide (CO_2) carbon monoxide (CO), and black carbon (BC) were also measured simultaneously at a frequency of 60 s. The filters collecting the PM mass in five different size ranges ($PM_{>10}$, $PM_{2.5–10}$, $PM_{2.5–0.1}$ and $PM_{<0.1}$) were exchanged every 3 days. $PM_{2.5}$ was collected on 47 mm polytetrafluoroethylene (PTFE) and quartz fibre filters by mini volume samplers. These filters were analysed for trace metals size distribution and crystalline phase (characterised by scanning electron microscopy (SEM)/transmission electron microscopy (TEM)) and x-ray ray diffraction (XRD), elemental and organic carbon, respectively and for polycyclic aromatic hydrocarbons (PAHs) (characterised by gas chromatography–mass spectrometry (GC–MS)) (Section 2.5). $PM_{>10}$, $PM_{2.5–10}$, $PM_{0.1–2.5}$ were collected onto polyurethane foams (PUF) that were analysed for trace metals using Harvard impactors (Section 2.5). $PM_{<0.1}$ were collected on 47 mm PTFE filters using Harvard cascade impactors. These filters were analysed for PM size, composition and crystal phase by TEM (Section 2.5 and Supplementary Sections S1, S2 and S3).

2.1. Site description

South Kensington station serves the District, Circle, and Piccadilly lines, with a train frequency of every 2–6 min for the District line, 8–12 min for the Circle Line, and 2–6 min for the Piccadilly line (TfL, 2020). District and Circle line trains use platforms 1 and 2 which are open to surface air and the Piccadilly line uses deeper platforms (3 and 4) which are closed off from surface air. The field campaign to monitor airborne concentrations

and sample the PM mass were carried out from 29 September 2020 to 22 October 2020 on the Eastbound platform #4 of South Kensington station of the Piccadilly line (Fig. 1) during both operable hours (OpHrs) (05:00 to 00:00 h; local time) and non-operable hours (N-OpHrs) (00:00 to 05:00 h). The Piccadilly line in South Kensington station is around 18 m deep and 3.6 m wide and is one of the busiest lines in the London underground with a footfall of ~33.86 million passengers per annum (TFL, 2020). Ventilation shafts extract air and act as a ventilation system for the station (COMEAP, 2018). These lines have been in service for more than a century. This station is a hub for many nearby cultural, professional, and public service institutions, resulting in high footfall throughout the day.

2.2. Airborne PM monitoring

Airborne PM mass concentrations were measured using a GRIMM (model 11-C) aerosol monitor (GRIMM Technologies Inc., Germany). This instrument measures particle size diameters of PM_{10}, $PM_{2.5}$ and PM_1 in 31 different, equidistant size channels at a size range of 0.25–32 μm particles at a flow rate of 1.2 L min^{-1}. We used a sampling interval of 60 s to measure the airborne concentrations of PM_1, $PM_{2.5}$, and PM_{10}. This equipment has been widely used for PM concentration measurements in previous studies (Abhijith and Kumar, 2019; Rivas et al., 2017b). The instrument ran continuously for 24 h each day for the entire sampling period. The measured data were downloaded from the instrument once every 3 days and visualised using the GRIMM Aerosol Technik (V8–1 Rev. IV) software. Furthermore, the visualised raw data were imported into the software and processed to obtain the airborne concentrations.

The CO_2 and CO concentrations, temperature, and relative humidity were measured using a QTrak monitor (model 7575-X, TSI Inc., USA). The QTrak uses a dual-wavelength NDIR (non-dispersive infrared) sensor, which measures CO_2 concentrations in the range of 0 to 5000 ppm with an accuracy of ±3.0 % or ± 50 ppm, whichever is greater. Additionally, the CO_2 concentrations, CO, temperature, relative humidity, and barometric pressure measurements were measured, and data was extracted once every 3 days, using the TrakPro™ Data Analysis software, which visualises the data and exports for further analysis.

BC measurements were monitored using a portable MicroAeth MA200 monitor (Aethlabs, USA), operating at a flow rate of 0.1 L min^{-1} without using an inlet cyclone. The data was extracted once every 3 days during the sampling period. The recorded measurements were then extracted using USB connectivity to cross-platform microAeth® Manager software that facilitates setting configuration and data downloading. The exported data was then uploaded to the AethLabs Dashboard server for processing and visualization. Attenuation of BC data generated due to instrumental optical and electronic noise was rectified by post-processing the data with the Optimized Noise-reduction Averaging algorithm (Hagler et al., 2011). The MA200 monitor uses a filter tape cartridge with 17 sampling locations of 3 mm diameter spots created on filter tape with a measurement resolution of 0.001 μg BC m^{-3}.

The Electrical Low Pressure Impactor (ELPI+, manufactured by DEKATI) is a real-time particle spectrometer used to measure airborne PND, in real-time, for a range of 0.006–10 μm with a flow rate of 9 L min^{-1} operated at an ambient temperature of 10–35 °C and relative humidity (RH) of 0–90 %. It has a pump pressure of 40 mbar, a charger voltage of 3.5 ± 0.5 kV and charger current of 1 μA. The charged particles collected in a specific impactor stage produce an electrical current, which is recorded by the respective electrometer channel. The sensitivity of ELPI+ for PNC is better for larger-sized particles as the amount of charge carried by a larger particle is significantly higher than one. For instance, the minimum detection limit of ELPI+ for 6 nm diameter particles is 250 # cm^{-3} which improves to 0.10 # cm^{-3} for 10,000 nm diameter particles. All the air quality monitors used in this study have a logging interval of 60s and a list of monitors used for data collection is mentioned in Table S1. The description on the performance of portable research-grade instruments can be found in SI Section S4.

2.3. Sampling of airborne PM

Two MiniVOL samplers (Airmetrics, Springfield, OR, USA), a Harvard Impactor, and ELPI+ were used for collecting the mass of size-segregated particles. Two MiniVOL samplers were used simultaneously to collect particles onto two different types of filters for performing chemical analysis. The filters were weighed before and after use to estimate the amount of particles collected and expressed in μg m^{-3}. Two MiniVOL samplers were used simultaneously to collect particles onto two different types of filters for performing chemical analysis. The first MiniVol sampler collected PM2.5 using a $PM_{2.5}$ impactor drawing air in at a flow rate of 5 L min^{-1} onto a 47 mm Polytetrafluoroethylene or Teflon (PTFE) filter

Fig. 1. (a) South Kensington Underground Station, Piccadilly line eastbound platform #4. (b) Air sampling equipment was placed on the station platform.

(TISCH Scientific #SF18040, with 2 μm diameter) and the second used a 47 mm quartz filter (WhatmanTM QMA grade).

The Harvard Impactor operates at a flow rate of 30 L min^{-1} using three different impaction stages which collect size-fractionated particles of PM_{10}, $PM_{10-2.5}$ (coarse), and $PM_{2.5-0.1}$ (fine) on PUF (Merryweather Foam, OH), with a thickness of 0.64 cm and a density of 20 kg m^{-3}. Particles in the size range ≤100 nm ($PM_{0.1}$) were collected on 47 mm Teflon (PTFE) filters (TISCH Scientific #SF18040, with 2 μm diameter). The ELPI+, used to examine the number concentration and number size distribution for the particle size range of 0.006–10 μm, was operated at a flow rate of 9 L min^{-1}. In addition, the instrument collected particles onto polycarbonate filters. Prior to sampling, quartz filters were baked at 550 °C for 12 h to remove any artefacts. They were weighed before and after sampling using a microbalance (Mettler Toledo XPR10) with a sensitivity of ±1 μg. After sampling, the filters were sealed in aluminium foil bags and stored in a freezer (−20 °C) prior to analysis. All the sampling filters were collected every 3 days and stored at a temperature of 4 °C until further analysis.

2.4. Data analyses

The data collected by the air monitors (GRIMM, Q-Trak, microAeth and ELPI+) at a sampling frequency of 60s was combined. The final dataset consisted of temperature, relative humidity, CO_2, PM_{10}, $PM_{2.5}$, PM_1, BC, particle size distribution and concentration. The secondary variables such as $PM_{10-2.5}$, PM_1/PM_{10}, $PM_{2.5}/PM_{10}$, particle number concentration (PNC) size range contribution from these datasets were estimated. The microAeth collects a wide range of particle sizes. However, the BC measurements are only of the light-absorbing particles of the sample, which are typically 0–1 μm in diameter. All the analyses were carried out using R software (v4.0.3) (R Core Team, 2020), the open-air package (Carslaw and Ropkins, 2012), and Python software (v2.7) (Python Core Team, 2018).

We generated a train schedule recording the moment when the front of the trains entered the platform area (i.e., train still moving, not stationary on the platform). This data was collected manually and in accordance with COVID guidelines on social distancing. Therefore, data collection took place in the following periods (avoiding busy station times): 12:30–14:03 h, 14:26–15:00 h and 15:54–17:00 h on 22 October 2020. A dichotomous variable was created taking the value of 1 if a train arrived at the station, otherwise 0. The train schedule was also included in the main dataset by means of the dichotomous variable, and populated only when data was available. Based on this information, point biserial correlations (r_{pb}) between aerosol (mass and number) concentrations and train arrival were calculated. Similar analysis has been used by other studies (Xiao et al., 2015; Griebel et al., 2019). The SciPy v0.18 open-source software for scientific computing in Python was used for this purpose.

2.5. Physico-chemical imaging and analyses of the PM

We combined complementary experimental techniques to characterise the composition of metals and organics in the PM. In summary, SEM combined with energy dispersive x-ray spectroscopy (EDXS) was performed to observe the morphological characteristics and chemistry of $PM_{2.5}$ and PM_{10}. The morphology and chemistry of fine and ultrafine PM fractions were characterised using transmission electron microscopy (TEM) combined with EDXS and scanning transmission electron microscopy (STEM) combined with EDXS. Full details of the extraction procedures and electron microscopy techniques used, and information they provide, are described in SI Sections S1, S2 and S3 and summarised schematically in Fig. S2.

XRD was used to characterise the crystalline phases in the PM. A PANalytical X'pert Pro Multi-Purpose Diffractometer with a Cu anode was used to examine PM evaporated on a Si wafer. The sample was scanned for 16 h with a step size of 0.0334^0 from 0 to 100^0 at room temperature. Spectra collected by Ferreira, Travar, Hamdan and Alawadhi (Ferreira et al., 2006; Travar et al., 2015; Hamdan and Alawadhi, 2020) were used as a reference.

For inductively coupled plasma mass spectrometry (ICP-MS) analysis, particle extraction from size-fractionated PUF ($PM_{2.5-0.1}$, $PM_{10-2.5}$ and $PM_{\geq 10}$) was conducted in Milli Q (Merck, Millipore) water with pulse sonication. IC-MS was performed using 2 sets of 3 filters (size-fractionated Polyurethane filters, i.e., 6 filters in total). Particles were dried and digested in acid, after which the remaining carbon was removed by centrifugation. Measurements were taken on Perkin Elmer NexION 350D Inductively Coupled Plasma Quadrupole Mass Spectrometer (ICP-QMS) at the London Metallomics Facility, King's College London. For organic compound analysis, a quarter of the PTFE filter was placed in a test tube and spiked with an internal standard (d8-naphthalene) then 1 mL of dichloromethane was added. The sample was extracted in a sonic bath, followed by centrifugation and the supernatant was transferred to a clean test tube. The procedure was repeated four times and the supernatants were combined. The extract was filtered through quartz wool held in a pipette to remove any particulates and the eluant was reduced in volume under a stream of nitrogen to ~50 μL for analysis by GC–MS.

GC–MS analysis was carried out using an Agilent Technologies 7890A GC coupled to a 5975C MS. The GC injector was operated in split mode (10:1) with a column flow rate of 1.1 mL min^{-1}. A J&W scientific DB-5MSUI capillary column (30 m, 250 μm i.d., 0.25 μm film thickness) was used for separation and helium employed as a carrier gas. The GC oven temperature was initially held at 40 °C for 2 min, and then raised to 310 °C at a rate of 5 °C min^{-1} where it was held for 14 min. Mass spectra were acquired in electron impact mode (70 eV) in the scan range of 50–500 amu and also in selective ion monitoring for quantitation of aromatic hydrocarbons and polycyclic aromatic hydrocarbons (PAHs). For quantification, an internal standard was added at the start of the procedure that was self-correcting for any losses during extraction. For our GC–MS method, the limit of detection (LOD) and limit of quantification (LOQ) were approximately 2 pg and 4 pg injected respectively for PAH in the low molecular weight range from naphthalene (*m/z* 128) to pyrene (*m/z* 202). For higher molecular weight PAHs, the LOD and LOQ were better than 4 pg and 10 pg injected, respectively. The LOQ equates to better than 0.005 ng/m^{-3} for the lower molecular weight range PAHs and 0.01 ng/m^{-3} for the higher molecular weight range PAHs.

2.6. Underground ventilation

The decay approach was used to calculate the air change rate (ACH; h^{-1}), which quantifies the number of times per hour that air is replaced by outdoor air, using the measured CO_2 concentration in the underground platform. The decay method has been used by other researchers for school ventilation studies (Canha et al., 2016; Hänninen, 2013; Ramalho et al., 2013). The selected approach is related to the CO_2 decay sequence when the concentration decreases towards the background level following Eq. (1):

$$C(t) = (C_0 - C_R)e^{-ACH\ t} + C_R \quad (1)$$

where C(t) is the concentration at time t (h); C_0 is the initial concentration; C_R is the CO_2 concentration in the replacement air. In addition, assuming a homogeneous CO_2 distribution, the ACH is proportional to the CO_2 concentration in the underground platform according to Eq. (2):

$$ACH = -\frac{1}{\Delta t}\ \ln\left\{\frac{C_1 - C_R}{C_0 - C_R}\right\} \quad (2)$$

where Δt is the time (h) between initial (C_0) and final (C_1) observed concentrations. The ACH was calculated with a 10-min average CO_2 data. Decay sequences meeting all of the following three criteria were selected to obtain the ACH: (i) Sequences using a time window of 8-h; (ii) The concentration change (ΔCO_2) between C_0 and C_1 of >50 ppm (over the typical instrument accuracy); and (iii) When each identified sequence is compared with Eq. (2) using the determination coefficient (R^2) and those giving $R^2 \geq 0.9$ were selected.

2.7. Exposure doses

Exposure to PM and ultrafine particles poses potential health risks. Air pollution inhalation exposure is determined here using estimated respiratory deposition dose (RDD) rates. The total dose received by an individual equals the difference between the number of particles inhaled and exhaled during each breath, breathing rate and the duration of exposure (Azarmi et al., 2014; Joodatnia et al., 2013). The RDD is significantly influenced by the size, shape, density and mass of the particles. Particle deposition and inhalation rate through respiratory tracts are estimated using algebraic and semi-empirical deposition models (Hofmann, 2011). We adopted a deposition fraction (DF) model (ICRP, 1994) of the International Commission on Radiological Protection (ICRP) since it is a commonly used approach by researchers (Keast et al., 2022; Martins et al., 2015b) and in our previously published work (e.g. Abhijith and Kumar, 2021; Kumar et al., 2018; Kumar and Goel, 2016). The RDD for mass and number concentrations are expressed in terms of the mass of particles deposited per unit time ($\mu g\ h^{-1}$) and the number of particles deposited per unit time ($\#\ h^{-1}$), respectively. Mass-based RDD for PM_{10}, $PM_{2.5}$ and PM_1 are estimated using Eq. (3).

$$\text{RDD of PM (different size fractions, } i) = (V_T \times f) \times DF_i \times PM_i \quad (3)$$

where V_T represents the tidal volume of humans, f is the breathing frequency, DF_i is the deposition fraction of particle size i in μm and PM_i is the mass concentration of particle size i in μm. V_T value varies according to gender and type of activity being carried out. In the case of the underground environment, we assume the human subjects are performing light exercise (Martins et al., 2015b) and the corresponding values of V_T as 1.25 L for males and 0.992 L for females and f as 20 and 21 min^{-1} for males and females, respectively. Usually, the total deposition fraction (DF_i) is estimated using Eq. (4) for the mass median diameter (d_p) of PM_{10}, $PM_{2.5}$ and PM_1 (Hinds, 1999). The d_p for different PM fractions (PM_{10}, $PM_{2.5}$ and PM_1) were calculated using the mass concentrations of each size bin (Kumar et al., 2021; Kumar et al., 2018) and subsequently, a plot has been made between the cumulative mass percentage of PM for different size fractions against the particle diameters (Fig. S3). The d_p was then determined by observing the 50 % of cumulative mass percentage to the corresponding particle diameter. RDD's for both particle mass concentrations (PMCs) and particle number concentrations (PNCs) were calculated using the DF_i values extracted from the average data of males and females for total and regional deposition for light exercises predicted from the ICRP deposition model (Hinds, 1999) for different regions of the human respiratory tract (HRT), which are the extrathoracic region (ET), tracheobronchial region (TB) and alveolar region (AL). The total deposition DF is the sum of these three regions or the DF can be expressed as mentioned in Eq. (4):

$$DF = IF \times \left(0.058 + \frac{0.911}{1 + \exp(4.77 + \ln d_p)} + \frac{0.943}{1 + \exp(0.58 - 2.58\ \ln d_p)}\right) \quad (4)$$

where IF is the inhalable fraction, which is calculated using Eq. (5):

$$IF = 1 - 0.5\left(1 - \frac{1}{1 + 0.00076 d_p^{2.8}}\right) \quad (5)$$

Similarly, the RDD for PNCs has been calculated using Eq. (6).

$$RDD\ of\ PNCs\ (Size - dependent\ DF) = (V_T \times f) \sum_{i=1}^{14} PNC_i \times DF_i \quad (6)$$

where PNC_i and DF_i are the particle number concentration and deposition fraction of particles in each size range (i), respectively. Subsequently, these doses have been summed up according to the particle modes as nucleation (N_{6-30}), accumulation (N_{30-300}) and coarse ($N_{300-10000}$).

3. Results and discussion

3.1. Overview of particle number and mass concentrations

Table S3 shows the summary statistics of all the data recorded during the field campaign. Fig. 2 shows the summary of aerosol mass concentration and the ratio of all the data collected over the 24-h period across all the monitoring days, including weekdays and weekends (hereafter referred to as full data) and segregated during underground non-operational hours (N-OpHrs, 00:00 to 05:00 h; local time) and operational hours (OpHrs, 05:00 to 00:00 h). Overall, the $PM_{2.5}$ and PNC concentrations ranged from 7.4 $\mu g\ m^{-3}$ (10th percentile, P10) to 69.3 $\mu g\ m^{-3}$ (90th percentile, P90), and from 3070 cm^{-3} (P10) to 17,151 cm^{-3} (P90), respectively. The concentrations of underground PM_{10} and $PM_{2.5}$ during OpHrs are ~5 times higher than that of the concentrations of roadside environments (PM_{10}; 22 $\mu g\ m^{-3}$) and ($PM_{2.5}$; 14 $\mu g\ m^{-3}$) in London (DEFRA, 2021). The concentrations measured in the current study are lower than the $PM_{2.5}$ (270–480 $\mu g\ m^{-3}$) and PNC (14,000–29,000 cm^{-3}) concentrations reported by Seaton et al. (2005) at three London underground stations (Holland Park, Hampstead and Oxford Circus). Such concentration differences could be due to factors such as the age of the line, trains in use, construction technique, passenger density and station depth (Hester and Harrison, 2009). However, the reported value of $PM_{2.5}$ (52 $\mu g\ m^{-3}$) by Smith et al. (2020) for the Piccadilly line inside the subway train and 68 $\mu g\ m^{-3}$ by Saunders et al. (2019) for the shallow lines of the London underground network is within the range to those observed in our study. In addition, PM_{10} (52 $\mu g\ m^{-3}$) and $PM_{2.5}$ (34 $\mu g\ m^{-3}$) (Fig. 2a) concentrations over the full data were above the 24-h averaged World Health Organization (WHO) Air Quality Guidelines of PM_{10} (45 $\mu g\ m^{-3}$) and $PM_{2.5}$ (15 $\mu g\ m^{-3}$) (WHO, 2021). Such high concentrations represent a health risk to the users and staff of the London Underground.

The geometric mean concentrations of PM_1 (16.3 $\mu g\ m^{-3}$), $PM_{2.5}$ (33 $\mu g\ m^{-3}$), $PM_{2.5-10}$ (16 $\mu g\ m^{-3}$) and PM_{10} (49.9 $\mu g\ m^{-3}$) during OpHrs are about four-times higher than those obtained during N-OpHrs (4.7, 8.6, 3.5, and 12.9 $\mu g\ m^{-3}$, respectively) (Table S3). In particular, these results showed an increase of 3.5, 3.9, and 3.9-times the concentrations of PM_1, $PM_{2.5}$ and PM_{10}, respectively, when compared to OpHrs. In particular, the coarse fraction ($PM_{2.5-10}$) exhibited the highest increase of 4.5-times during OpHrs compared with N-OpHrs, confirming the importance of the aerosol settling process during N-OpHrs (Mugica-Álvarez et al., 2012).

Our PM fraction results differ from those reported by Mugica-Álvarez et al. (2012), who reported a geometric mean $PM_{2.5}/PM_{10}$ ratio of 0.56 ± 0.09 for the Azcapotzalco Underground Station in Mexico City. We obtained a slightly higher ratio of $PM_{2.5}/PM_{10}$ (0.66 ± 0.1) and $PM_{2.5-10}/PM_{10}$ (0.31 ± 0.1) using the full data; both these ratios were generally constant throughout OpHrs (Table S3). This suggests that, on average, the coarse fraction (0.31 ± 0.1; $PM_{2.5-10}/PM_{10}$) could be related to aerosol resuspension caused by train movement. Such fraction differences can be related to the underground station characteristics (e.g., ventilation settings, depth, and age of the tunnels), as mentioned by Smith et al. (2020). In terms of age, Azcapotzalco Station opened in 1989 (STC, 2022), and South Kensington Station between 1865 and 1870 (LTM, 2022). This operating period difference of around 124 years means that the tunnel designs are different as are the kinds of trains operating through time (early London underground trains were coal-fuelled steam trains for example). Additionally, compounded by low ventilation rates, huge amounts of dust will have accumulated throughout the years in South Kensington Station compared to Azcapotzalco Station.

The geometric mean concentration of BC (14.5 $\mu g\ m^{-3}$) during OpHrs were ~21-times higher than those (0.7 $\mu g\ m^{-3}$) during N-OpHrs (Table S3), suggesting that BC-rich particles are affected by aerosol settling processes and the lack of BC sources during N-OpHrs. In particular, BC concentrations ranged from 0.4 $\mu g\ m^{-3}$ (P10) to 40.6 $\mu g\ m^{-3}$ (P90) with a median of 14.3 $\mu g\ m^{-3}$, which is ~4.2-times higher than the reported median value (3.38 $\mu g\ m^{-3}$) for the Brazil railway (ground-level platforms) by

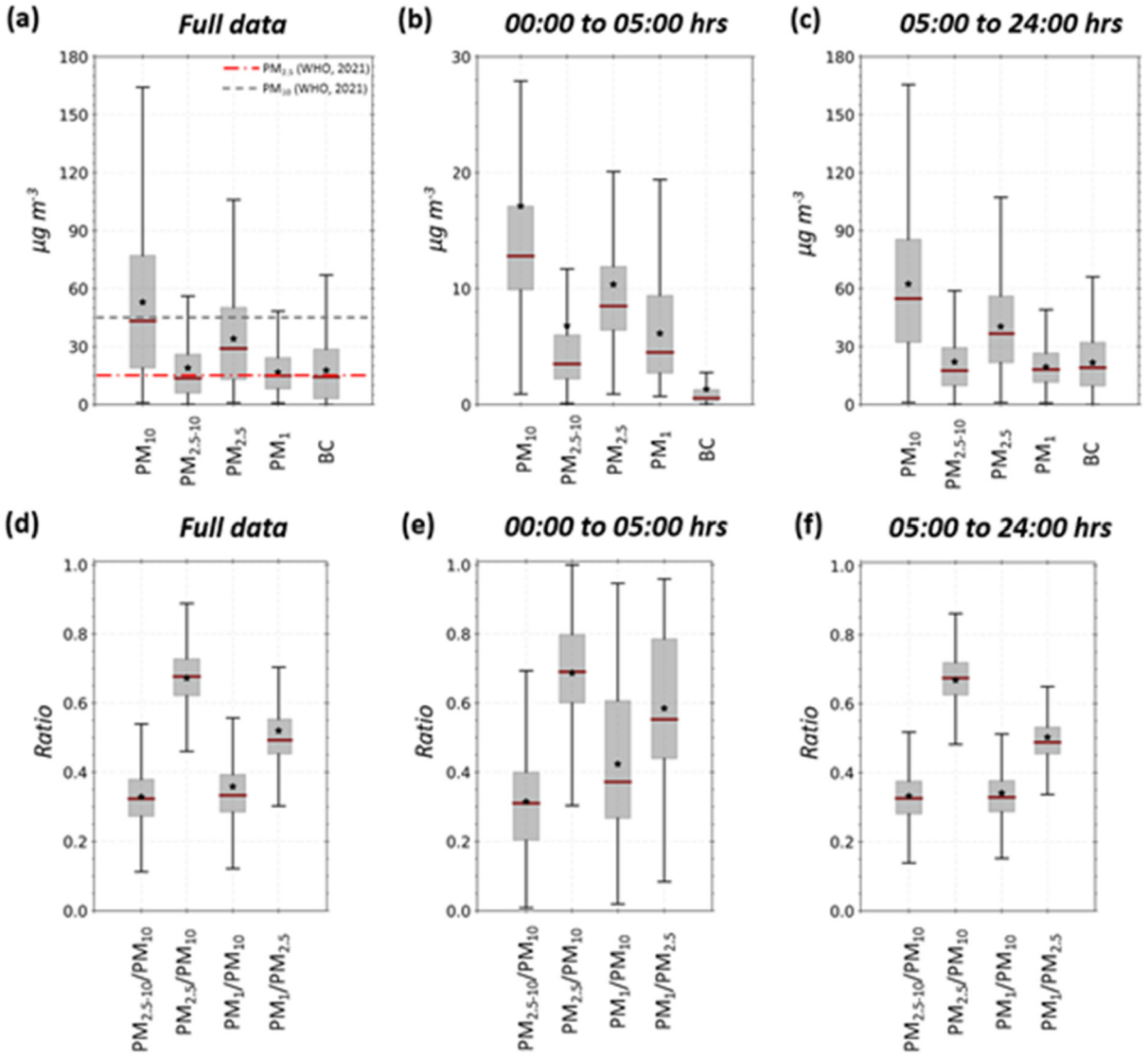

Fig. 2. Boxplots of (a-c) aerosol mass concentration and (d-f) aerosol mass ratios, for the full data (a, c), 00:00–05:00 h (b, e), and 05:00–24:00 h (c, f). Star symbols refer to arithmetic mean concentrations, while horizontal lines within the bars show the median values. Note that the y-axis of Fig. 2b is intentionally kept low (by a factor of six) to those in other sub-figures so that the bar plots are clearly visible.

Lima et al. (2021), and ~6.2-times the median value (2.3 ± 1.2 μg m^{-3}) for New York roadside (ground-level) by Vilcassim et al. (2014). However, the median value reported here is similar to those (14.0 ± 5.4 μg m^{-3}) reported for the West 4th subway upper level (New York, USA; Vilcassim et al., 2014). By contrast, BC geometric mean concentrations in our study are around 31 % lower than those observed in the West 4th subway lower level (20.9 ± 3.8 μg m^{-3}) by Vilcassim et al. (2014). This could be related to the spatial variation, depth of the station and underground line sampled (Vilcassim et al., 2014) and, during our study, the COVID-19 pandemic reduced the users of the London underground by ~64 ± 3 % with respect to 2019 (DfT, 2021), but not the train frequency during the sampling campaign.

Fig. S4 shows that PM_1, $PM_{2.5}$, PM_{10} and BC concentrations (full data) are similar during weekdays. Moreover, a similar pattern (during weekdays) was observed for PNC (Fig. S5). By comparison, a significant decrease ($p < 0.05$) was observed during weekends, with reductions of −15 % for PM_1, −22 % for $PM_{2.5}$, −26 % for PM_{10}, −20 % for PNCs, and − 22 % for BC compared with weekdays.

Heatmaps of hourly PM_1, $PM_{2.5}$, PM_{10} and BC (Fig. S6) illustrate the contrast between N-OpHrs and OpHrs, where high concentrations are mainly observed during OpHrs. In particular, N-OpHrs exhibited no significant differences ($p < 0.05$) between weekdays and weekends, for both BC and PM_1 concentrations, with an increase of +1 % for BC, and a reduction of −2 % for PM_1. By contrast, $PM_{2.5}$, PM_{10} and PNC showed a significant decrease, with reductions of −17 % for $PM_{2.5}$, −29 % for PM_{10}, and − 35 % for PNC. During OpHrs significant differences ($p < 0.05$) between weekdays and weekends were observed for PM_1, $PM_{2.5}$, PM_{10}, PNC and BC, with reductions of −16 % for PM_1, −22 % for $PM_{2.5}$, −25 % for PM_{10}, −16 % for PNCs, and − 23 % for BC. Such differences could be related to a reduction in the number of passengers and lower train frequency during weekends (Mugica-Álvarez et al., 2012). Overall, the PM pollution in the studied London underground platform exhibits the following trend: weekday OpHrs > weekend OpHrs, and weekday N-OpHrs = weekends N-OpHrs.

3.2. PM mass concentration

Fig. 3a–d show the diurnal variation using the full data, where considerable PM_1, $PM_{2.5}$, PM_{10} and BC concentration differences were measured between N-OpHrs and OpHrs. PM_{10} and $PM_{2.5}$ showed two large peaks at around 07:00 h and 17:00 h. This increase can be related to the train frequency and numbers of passengers (morning and afternoon rush hour), as

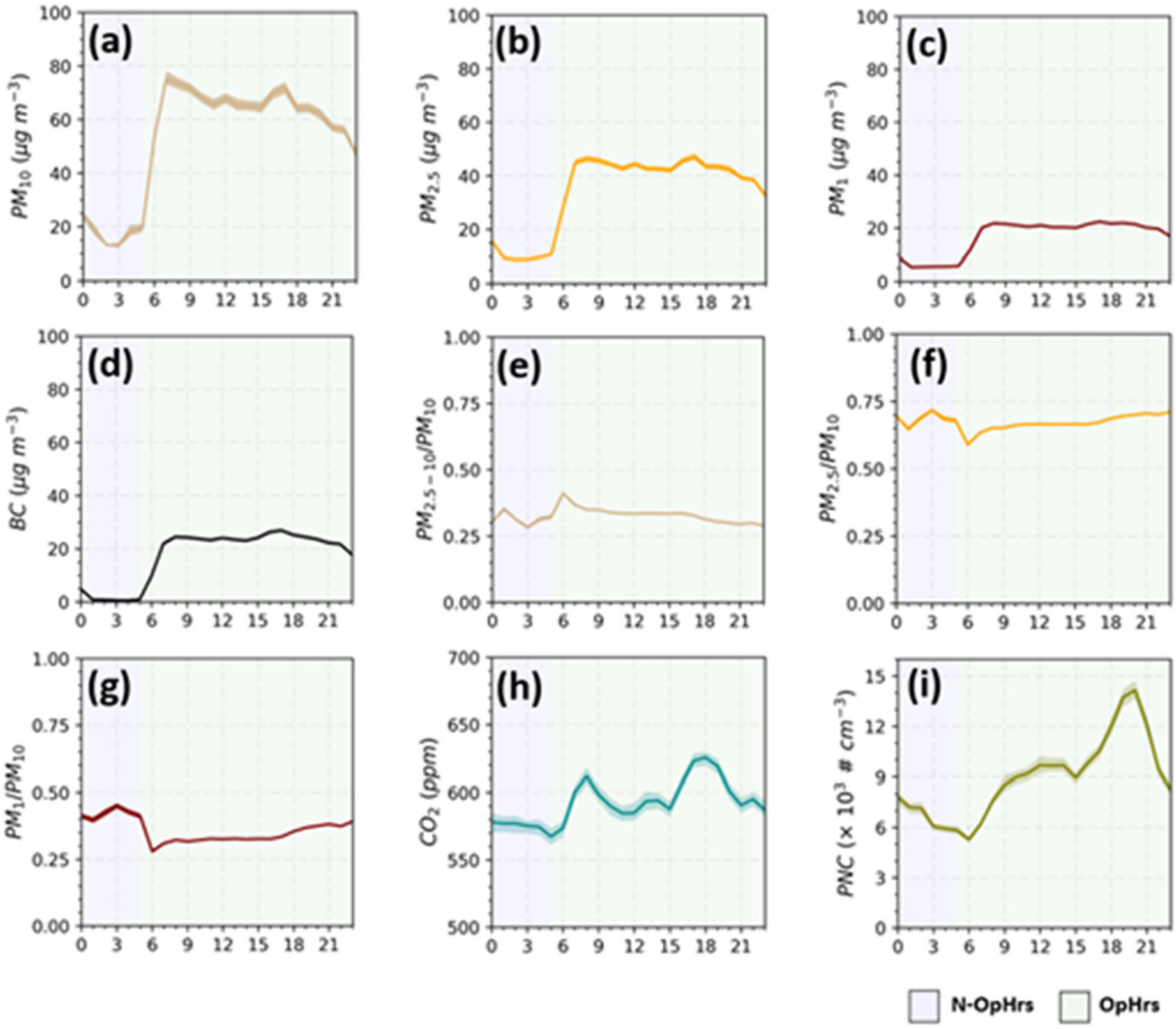

Fig. 3. Diurnal variation (1-h resolution) of (a) PM_{10}, (b) $PM_{2.5}$, (c) PM_1, (d) BC, (e) $PM_{2.5–10}/PM_{10}$, (f) $PM_{2.5}/PM_{10}$, (g) PM_1/PM_{10}, (h) CO_2, and (i) PNC measured at the UG site. X-axis represents time in hours and the shaded area indicates 95 % confidence intervals. Blue and green shaded areas represent the underground non-operational (N-OpHrs) and operational hours (OpHrs), respectively.

was also reported by Salma et al. (2007) for Budapest. For instance, the highest PM_{10} and $PM_{2.5}$ were ~781 μg m^{-3} and ~250 μg m^{-3}, respectively (Fig. S7). Both PM fractions increased rapidly during the transition from N-OpHrs to OpHrs (Fig. 3). Similar study results have been reported by Tu and Olofsson (2021) for the underground subway of Stockholm (Sweden) where the PM concentrations were found to possess a positive correlation between train frequency and platform PM levels for the various PM fractions (PM_{10}, $PM_{2.5}$ and PM_1).

The concentration of BC (1-min average peaks) reached ~86 μg m^{-3} (Fig. S8). The most plausible explanation for such high levels of BC could be that they have been originated from the underground related activities such as the emissions from graphite connections between the third rail and the trains (Van Ryswyk et al., 2017). Additionally, the presence of Fe particles in underground environments results in an overestimation of BC concentrations (Rivas et al., 2017a), which cause interference due to its absorbance of visible light at similar wavelengths (Moreno et al., 2015a; Gilardoni et al., 2011). In some cases, the use of diesel-powered maintenance trains in similar underground environments would have contributed to higher levels of BC as reported for New York city's subway station by Vilcassim et al. (2014), who recorded BC peaks of 111 μg m^{-3} when a diesel locomotive passed through the station. It is unlikely, however, that diesel-powered trains were in operation in our study area. The presence of Fe was demonstrated by the chemical composition analysis (Section 3.5), which shows that particles were mostly composed of Fe, and bulk composition analysis indicates around 23–76 % Fe by weight.

Although there is a decrease in PM_{10}, $PM_{2.5}$ and PM_1 between OpHrs and N-OpHrs, the average $PM_{2.5–10}/PM_{10}$, $PM_{2.5}/PM_{10}$ and PM_1/PM_{10} ratios (Fig. 3e–g) were almost constant throughout the day. $PM_{2.5}/PM_{10}$ and PM_1/PM_{10} ratios showed a maximum peak at 03:00 h (Fig. 3f–g); this behaviour indicates the settlement of $PM_{2.5–10}$, which has been reported in other studies (Mugica-Álvarez et al., 2012; Salma et al., 2007). Conversely, the maximum $PM_{2.5}/PM_{10}$ ratio of ~0.72 was observed between 00:00 and 05:00 h, which is lower than the value of 0.94 (when compared to N-OpHrs) reported by Mugica-Álvarez et al. (2012) and Raut et al. (2009). This indicates that some mass fraction of PM_{10} remains in the underground atmosphere, or there are some overnight activities (e.g., cleaning, maintenance) re-suspending or generating coarse particles (>2.5 μm) (Raut et al., 2009). For instance, Fig. 4a shows that on average the coarse fraction accounted for 36 % of the total PM_{10} mass, and during different hours of the day (Fig. 4b–i) could range between 31 % (21:00 h) and 47 % (06:00 h). In addition, we observed that PM_1 mass contribution to PM_{10} increased between 18:00 and 04:00 h, with a maximum peak of 43 % at 03:00 h (Fig. 4c), also indicating the settlement of PM_{10}.

Overall, Fig. 4j–k show that the contribution to PM_{10} increased from 31 % (OpHrs) to 36 % (N-OpHrs) and from 35 % (OpHrs) to 40 % (N-OpHrs) for PM_1 and $PM_{2.5–10}$, respectively. By contrast, the $PM_{2.5–10}$

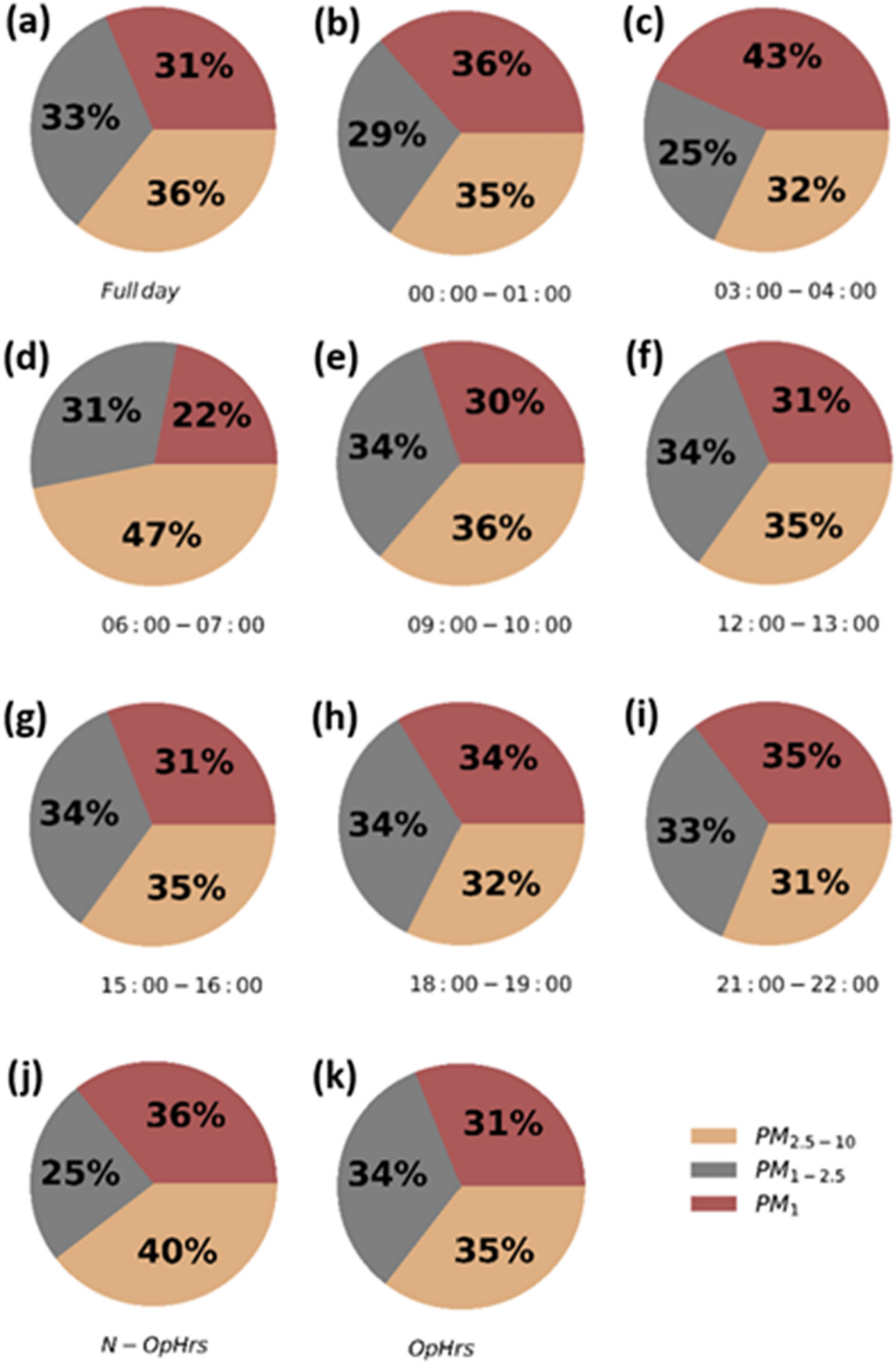

Fig. 4. Pie charts showing the contribution of PM fractions (PM_1, $PM_{1–2.5}$, $PM_{2.5–10}$) to total PM (full data) for (a) 24 h, (b) 00:00–01:00 h, (c) 03:00–04:00 h, (d) 06:00–07:00 h, (e) 09:00–10:00 h, (f) 12:00–13:00 h, (g) 15:00–16:00 h, (h) 18:00–19:00 h, (i) 21:00–22:00 h, (j) non-operational hours (N-OpHrs) and (k) operational hours (OpHrs).

contribution to PM_{10} increased from 25 % (N-OpHrs) to 34 % (OpHrs), which indicates that the aerosol fine fraction (<2.5 μm) contributions are similar between N-OpHrs and OpHrs, with values ranging from 61 % to 65 %, respectively.

Temporal variability at a one-minute resolution of PM_{10}, $PM_{2.5}$, PM_1, BC and CO_2 was evident in our experiment (Fig. S9), which is in good agreement with the findings of Tu and Olofsson, 2021, as well as of Cusack et al. (2015) who observed that the train frequency was more significant for PM variation in the underground tunnel.

3.3. Particle number and size distributions

The geometric mean of PNC (Table S3) during N-OpHrs (5315 cm^{-3}) and during OpHrs (7835 cm^{-3}) are comparable with those reported by Raut et al. (2009) in the Magenta subway station (Paris, France), who observed PNC levels of 7000 cm^{-3} during operational hours and 4000 cm^{-3} during non-operational hours. Our results differ from the observations made in Prague underground metro (Czech Republic) by Cusack et al. (2015), who reported higher levels than ours at 8500 cm^{-3} and 11,500 cm^{-3} for background and operational hours, respectively. In addition, the percent of change (PC = [(OpHrs – N-OpHrs)/N-OpHrs] × 100) was calculated using GM to compare our results with Raut et al. (2009) and Cusack et al. (2015). Our study indicates an increase of 47 % (between N-OpHrs and OpHrs) while the work by Raut et al. (2009) revealed an increase of 75 %. Conversely, an increase of 35 % was obtained by Cusack et al. (2015) using background levels as N-OpHrs. Those values indicated that PNCs increased during OpHrs could range from 35 % to 75 % of PNCs during N-OpHrs. Additionally, PNCs during OpHrs were 4.7-times lower than typical roadside environments (2.5×10^4 cm^{-3}) (Kumar et al., 2021).

Fig. 5a shows the diurnal variation of PNC; the lowest concentrations were observed between 03:00 and 06:00 h, similar to PM_{10}, $PM_{2.5}$ and PM_1 patterns (Fig. 3a–c). By contrast, the maximum PNC peaks were observed at different times between 18:00 and 21:00 h than those observed in mass concentrations (07:00 and 17:00 h); this PNC behaviour is discussed in the subsequent text.

The daily average PND (Fig. 5b) shows a maximum peak between 6 and 30 nm (nucleation mode), and a slight peak between ~30 and 300 nm (accumulation mode). Our results are similar to those reported by Seaton et al. (2005) from a London underground study, who reported that 80 % of particles had <1 μm diameter using a microscopic measurement approach. Different hours were selected to compare the PND development (Fig. 5a). Over 70 % of the PNCs were found in nucleation mode between 03:00 and 06:00 h (Fig. 5c–d). By contrast, between 09:00 and 18:00 h, nucleation and accumulation mode particles accounted for 64 % and 33 % of the total PNCs, respectively (Fig. 5e–g). Additionally, PNCs observed during N-OpHrs could be related to the entrainment of surface air into the underground station and overnight activities (such as maintenance operations).

Overall, Fig. 5h shows that up to 70 % of the PNCs were observed in nucleation mode during N-OpHrs and decreased by 6 % to about 64 % of the total PNCs during OpHrs. We observed that PNDs during both N-OpHrs and OpHrs were similar, between 6 and 15 nm, and on average only larger particles showed a reduction during N-OpHrs; this behaviour aligns well with PNDs reported by Raut et al. (2009) during operational and non-operational hours. Moreover, during OpHrs, the particle mass distribution (PMD) shows an increase of particles (>0.1 μm) with a peak around 3 μm, representing an increase of just ~1 % of the PNCs in the coarse fraction (300 nm and 10 μm). The most plausible explanation for such behaviour is that in the underground environment most particles are submicron sized, but the mass concentration is governed by a small number of coarse particles (Raut et al., 2009).

Fig. 6 shows the variation of PNDs, PNC and $PM_{2.5}$ (from ELPI+) during field measurements. In particular, the transition between N-OpHrs and OpHrs is characterised by a sudden increase in the mass concentration of $PM_{2.5}$, and a gradual rather than abrupt PNC increase. By contrast, the transition between OpHrs and N-OpHrs (18:00 to 00:00 h) showed a mass concentration decrease at around 18:00 h, but PNC continued to increase, reaching a maximum concentration between 18:00 and 21:00 h (Fig. 6A–B). Cusack et al. (2015) and Seaton et al. (2005) reported a similar PNC pattern, which they related to the entrainment of surface air into the underground station.

The PND contours show that the particle size varies throughout the day (Fig. 6a); particles between 10 nm and 10 μm decreased during N-OpHrs, and an increase in particles between 10 and 300 nm was observed during OpHrs. The PNDs reported here show a peak of 126 nm, the same as results reported by Cusack et al. (2015), but we also observed high particle concentration between 6 and 20 nm, which is comparable with the results reported by Raut et al. (2009). We observed that PNC increased between 16 and 22 October 2020, with a maximum peak of 50×10^3 cm^{-3}. Similarly, Seaton et al. (2005), Raut et al. (2009) and Aarnio et al. (2005) reported PNC peaks up to 29×10^3 cm^{-3}, 20×10^3 cm^{-3} and 77×10^3 cm^{-3}, respectively. Such an increase was largely attributed to the entrainment of surface air to the underground platform (Aarnio et al., 2005; Seaton et al., 2005).

3.4. Ventilation

Table S3 shows the CO_2 concentrations, which ranged from 404 ppm (P10) to 740 ppm (P90) and reflects the variations in passenger numbers with a mean value of 558 ± 120 ppm (Fig. 3h). The CO_2 concentrations reported here are within the range of those reported by Moreno et al. (2015a, 2015b) in the Barcelona Subway (694 ± 63 ppm). Additionally, during our field measurements, the maximum CO_2 concentration observed was 936 ppm; a difference (ΔCO_2) of 525 ppm compared with the global (outdoor) average CO_2 mean (411 ppm; October 2020) (NOAA, 2021). Such an increase was largely attributed to the CO_2 generation caused by passengers and the ventilation conditions present in the underground environment. In addition, the diurnal variation of CO_2 shows two peaks; during the morning (07:00 h) and afternoon (17:00 h) rush hours (Fig. 3h), where CO_2 generation by underground users can be an important factor.

According to the American Society of Heating, Refrigerating and Air Conditioning Engineers (ASHRAE), the CO_2 concentration differences between indoor and outdoor air should be <700 ppm to be comfortable for occupants (ASHRAE, 2013). Adverse health effects (such as behavioural changes and physical stress) have been associated with CO_2 concentrations between 700 and 3000 ppm (Beheshti et al., 2018; Martrette et al., 2017). In our study, ~18 % of the CO_2 readings were over 700 ppm. However, as discussed in Section 3.1, occupancy of the London underground during the field measurements was about 64 ± 3 % lower than in 2019 due to the COVID-19 pandemic (DfT, 2021). As a result, the CO_2 present as a result of passenger exhalation can be assumed to be lower than would normally be expected.

Decay sequences that met the criteria explained in Section 2.4 can be found in Fig. S10. We observed that all sequences were detected after 17:00 h, which could be related to the decrease in occupancy due to the transition between OpHrs and N-OpHrs. This suggests that the ACH results could be related to outdoor air infiltration (Canha et al., 2016), but only if the ventilation system is turned off during N-OpHrs. The ACH varied between 0.17 and 0.46 h^{-1} (Table S2), with a mean value of 0.24 ± 0.11 h^{-1}. We observed the highest ACH value (0.46 h^{-1}) over the weekend (Saturday) and lower values during weekdays, which ranged from 0.17 h^{-1} to 0.23 h^{-1}. Similar findings had been reported elsewhere, where the platform air quality was reported to be improved during N-OpHrs and weekends due to factors such as the absence of trains, inhibiting resuspension and outside air by the train movements and allowing settling of resuspended particles (Tu and Olofsson, 2021; Moreno et al., 2015a, 2015b). There are no specific ACH limits for underground spaces, but as an example, these values are 50 % lower than the minimum recommended limit of 0.5 h^{-1} for Finnish residential buildings (Järnström et al., 2006). Moreover, the underground ACH is ~25-times lower than the recommended ACH in school classrooms (5–7 h^{-1}; VentAxia, 2021), 29-times lower than hospital ward guidelines (6–8 h^{-1}) (VentAxia, 2021), and

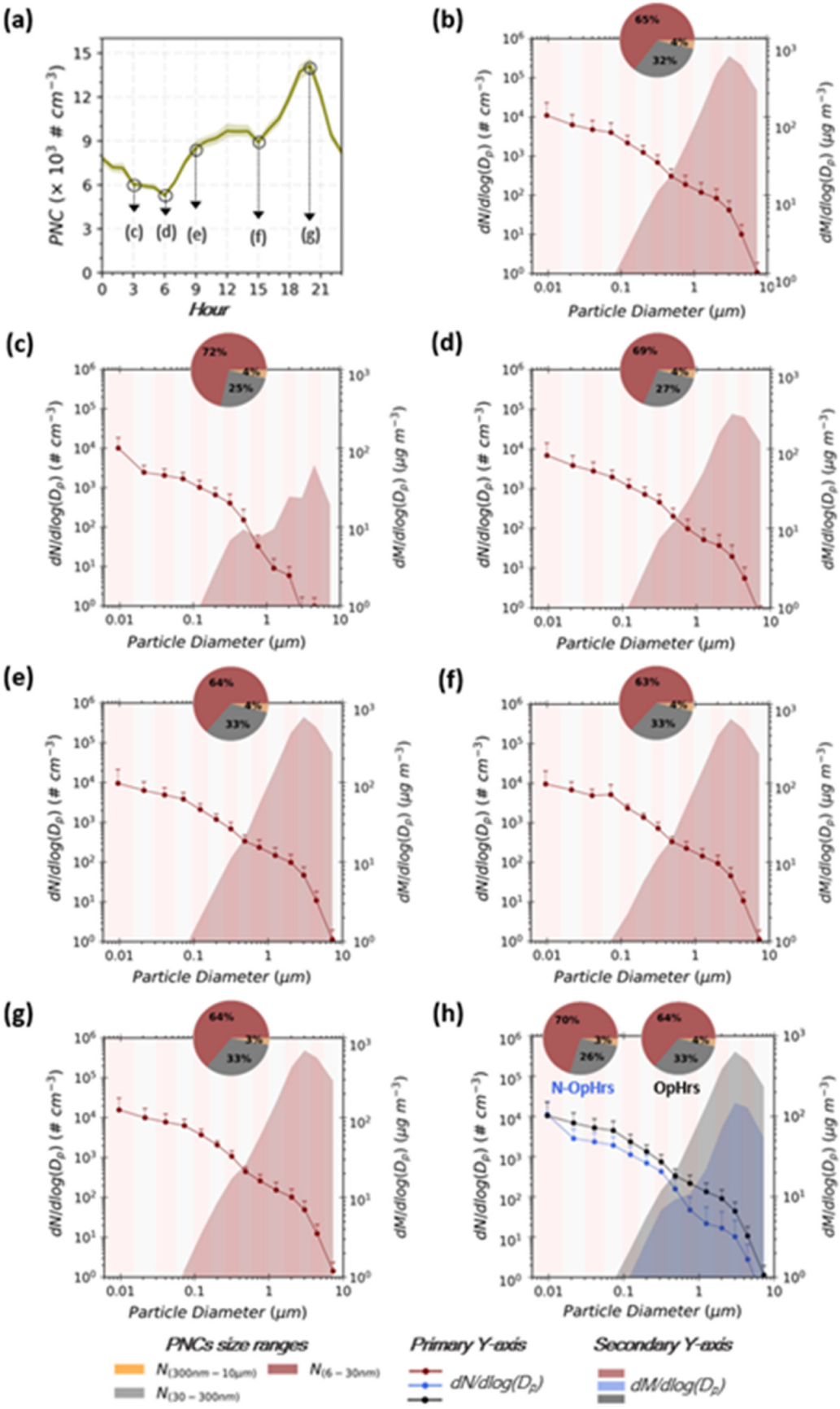

Fig. 5. (a) Diurnal particle number concentration variation, (b–g) particle number and mass distributions. In (b) average particle number and mass distributions using full data, in (c–g) showing different hours with a 1-h average window, and (h) during non-operational hours (N-OpHrs, blue color) and operational hours (OpHrs, black color). Pie charts represent the proportion of PNCs of different size ranges.

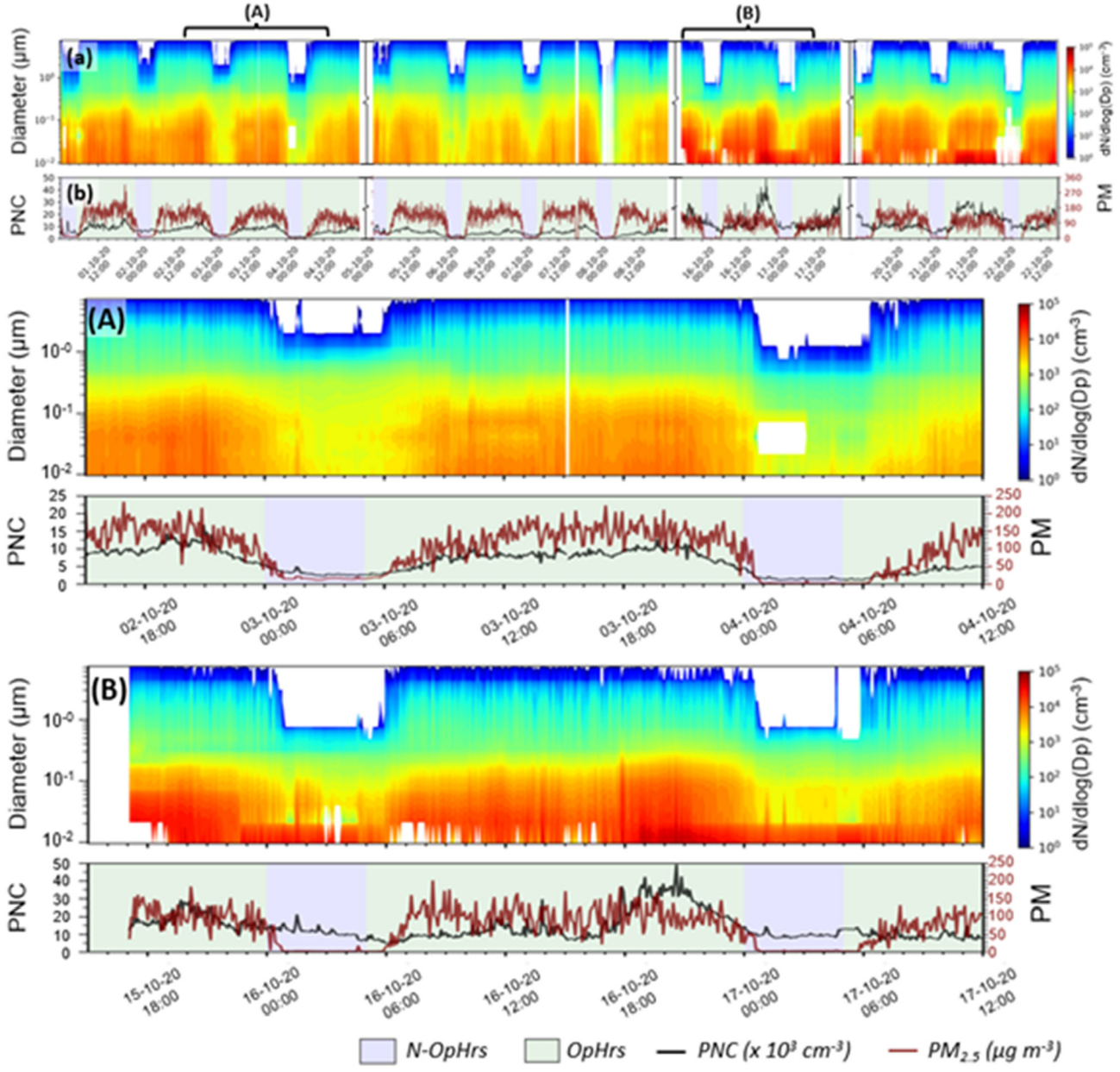

Fig. 6. Temporal variation of (a) PNDs, (b) PNCs and $PM_{2.5}$ during field measurements (top figure). Upper case letters A–B represent two selected time ranges. $PM_{2.5}$ was obtained using the ELPI+ macro file assuming a particle density of 1 g cm^{-3}. Blue and green shaded areas represent the underground non-operational (N-OpHrs) and operational hours (OpHrs), respectively.

~33-times lower than sport facility guidelines (6–10 h^{-1}; Ariëns et al., 2008; VentAxia, 2021).

Olesen and Parsons (2002) and the ISO 7730 guidelines recommend indoor temperature ranges of 22–27 °C for cooling (summer) and 19–25 °C for heating (winter) seasons. Ambient temperatures observed in the London underground ranged from 14.3 °C (P10) to 20.0 °C (P90), with a mean value of 15.1 ± 1.6 °C (N-OpHrs) and 17.8 ± 1.8 °C (OpHrs), Table S3. In addition, the mean temperature during N-OpHrs and OpHrs is below the recommended ranges, with ~78 % and ~99.9 % of the data below the inferior limit guidelines for heating and cooling seasons, respectively. Similarly, according to the ASHRAE Standard-55-2004, the indoor RH should be between 30 % and 60 % to avoid bacterial growth and skin irritation (Charles et al., 2005). In our study, the RH ranged from 49 % (P10) to 69 % (P90), with a mean value of 64 ± 6 % and 58 ± 8 % during N-OpHrs and OpHrs (Table S3), respectively, with 55 % of data within the recommended ASHRAE RH-threshold. Charles et al. (2005) note that comfortable temperatures are challenging to achieve with high RH values. Here, 45 % of RH values were over the upper ASHRAE threshold and could be linked with temperature values outside the ideal indoor ranges.

Fig. 7 shows the temporal variation of PM_1, $PM_{2.5}$, PM_{10}, PNC, temperature, and CO_2 between 06:00 and 12:00 h (01 October 2020). During those hours, the Spearman correlation of PM_1, $PM_{2.5}$, PM_{10}, PNC, and temperature with CO_2 was >0.4. A comparison between 07:00 and 08:00 h (Fig. 7a–e, A–E) showed a similar increase-decrease pattern with respect to CO_2. Those patterns suggest a CO_2-PM build-up/dilution loop related to the train movement through the underground platform, where: (i) during the time between trains, CO_2 levels start to increase (accumulation of people and CO_2 exhalation) combined with a slight rise in air temperature; (ii) when a train arrives at the platform, airborne PM levels increase through resuspension; (iii) when a train stops at the platform, all or some CO_2 sources are added/removed from the site; and (iv) the movement of the train leaving the platform could cause a rapid dilution process that affects PM and CO_2, causing a decrease of air temperature. In our study, train frequency data collected between 12:00 and 17:00 h on 22 October

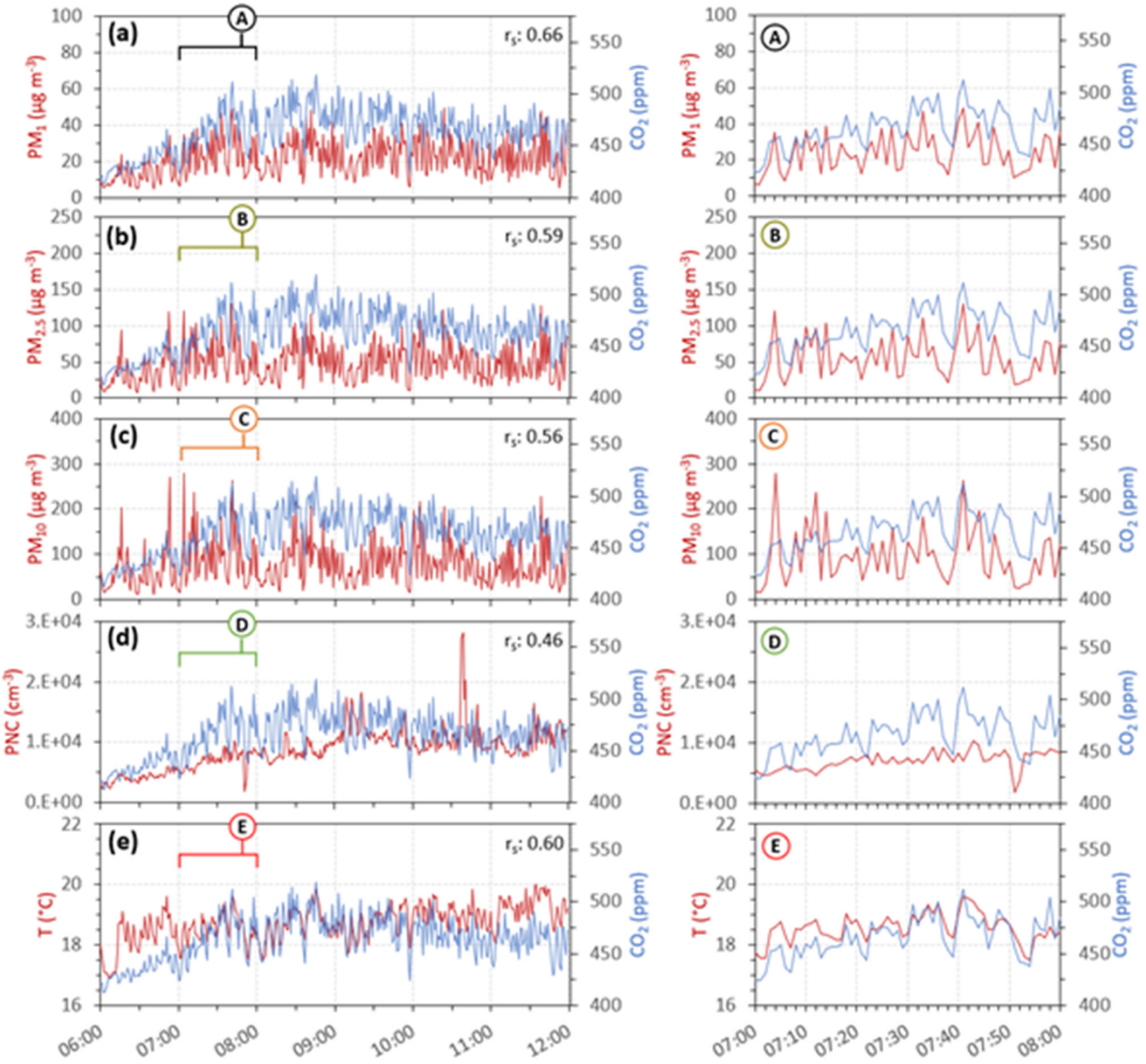

Fig. 7. Temporal variation (1-min resolution) between 06:00 and 12:00 h (October 01, 2020) for (a) PM_1; (b) $PM_{2.5}$; (c) PM_{10}; (d) PNC; and (e) Temperature. Spearman correlation (r_s) between each variable with CO_2 is indicated in the top right corner of each panel. ACH obtained for this day is (0.23 h^{-1}). Upper case letters A-E represent the selected time-window range (07:00–08:00 h).

2020 (Table S4), showed that trains arrived every 2.8 ± 0.9 min and spent around 1.0 ± 0.2 min at the platform, which suggests that approximately every 2.8 min a build-up/dilution loop occurs. For instance, using data collected between 12:00 and 17:00 h (22 October 2020), point biserial correlation coefficients (r_{pb}) indicated that PM_1, $PM_{2.5}$, PM_{10}, $PM_{1-2.5}$, and $PM_{2.5-10}$ were moderately correlated ($r_{pb} > 0.4$), and PNC weakly correlated ($r_{pb} = 0.02$) with trains arriving at the underground station (Table S5). Similar observations were made by Tu and Olofsson (2021), where positive correlations were found between train frequency and particle mass concentrations for PM_{10}, $PM_{2.5}$, and PM_1 particles. Fig. 8 shows the PM and PNC data points when a train arrived at the station. Our results suggest that only aerosol mass concentration (PM_1, $PM_{1-2.5}$, and $PM_{2.5-10}$) variations are positively correlated with trains arriving at the station. However, further measurements are needed to support our results under more detailed train frequency.

Negative or near zero Spearman correlations of PM_1, $PM_{2.5}$, PM_{10} and temperature with CO_2 were observed (−0.46 to −0.04) between (00:00 and 06:00 h) (Figs. S11–13), which is related to a PM decrease when compared to N-OpHrs. By contrast, a positive Spearman correlation of PNC and CO_2 was observed (~0.4) (Fig. S15), which could be related to the entrainment of surface air into the underground station and overnight activities (e.g., cleaning and maintenance).

3.5. Chemical composition and morphology of PM

Bulk elemental analysis of $PM_{2.5-0.1}$, $PM_{10-2.5}$ and PM_{10} was conducted by ICP-MS on PM that was extracted off filters collected on the 03 and 15 October 2020 to characterise the composition of metallic components of different size fractions in PM based on their concentrations (Table S3). This confirmed the presence of elements including Na, Mg, Al, P, K, Ca, Ti, Cr, Mn, Fe and Ni. Fe constituted the largest elemental contribution (depicted by pie charts in Fig. S16) as seen in previous work (Loxham and Nieuwenhuijsen, 2019; Smith et al., 2020). There was a similar proportion of Fe by weight in $PM_{2.5-0.1}$ and $PM_{10-2.5}$ but lower in PM_{10} for both days collected. Al and Mn were the next most dominant metals across all size fractions. The Fe and Mn were probably generated from frictional contact

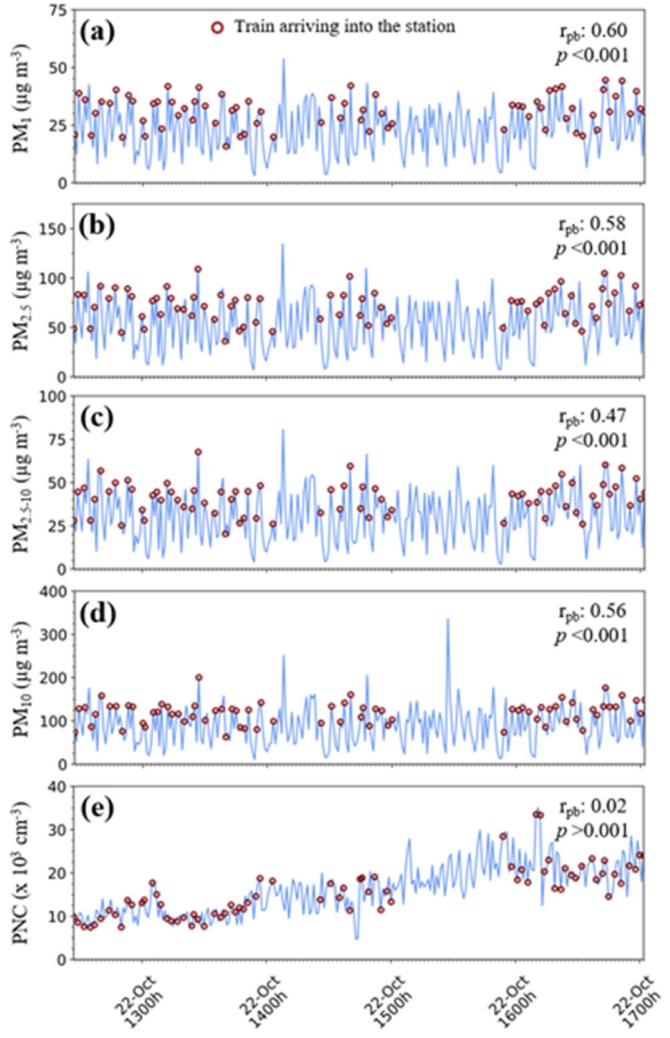

Fig. 8. Temporal variation (1-min resolution) for 22 October 2020 (between 12:30 and 17:00 h). (a) PM_1, (b) $PM_{1–2.5}$, (c) $PM_{2.5–10}$, and (d) PNC. The maroon concentration marked data point indicates train arrival. Point biserial correlation (r_{pb}) between each pollutant and trains arriving at the underground station, is indicated in the top right corner of each panel. Peaks outside the following time intervals 12:30–14:03 h, 14:26–15:00 h and 15:54–17:00 h were not labelled as train entering the station and not included in the analysis.

between the disc and pad of Fe-Mn-C steel braking systems, including the brake-wheel and rail-wheel interfaces (Bhadeshia, 2002; Moreno et al., 2015b). Trace toxic transition metals, notably Cr in the fine fraction, were present in the $PM_{2.5–0.1}$ fraction. Other metals were also detected, including Cu and Zn, also found in rail alloys and brake pads. We note that the sampling duration of 24 h was too long to collect and characterise large numbers of sampling events and hence precluding extensive statistical analysis, however, we are reassured by a number of characteristics. We assume that the underground train system represents a relatively stable atmospheric reservoir with consistent sources of PM, therefore the variability would be much lower than in a surface environment. Since we sampled for 24 h, all diurnal variables are captured in a single sampling event. We conducted these measurements and analysed this separately on two separate days and saw similar trends. This gives us confidence that the results are representative, although fine details may provide valuable opportunities for future studies.

XRD confirmed that the PM was composed of Fe-rich phases - in this case, quartz magnetite (Fe_3O_4) - and also sodium chloride (NaCl), quartz (SiO_2) and Gypsum ($CaSO_4 \cdot 0.5\ H_2O$) (Fig. 9a). Electron microscopy combined with spatially resolved EDX chemical analysis was used to characterise the distribution of elements and morphology of individual PM in each size fraction, including the ultrafine $PM_{0.1}$ (<100 nm) fraction (Figs. 9–10). Fig. 9 shows representative low-resolution ESEM images of PM (with a resolvable diameter distribution shown in (Fig. S17) on a polluted quartz filter with corresponding EDX chemical maps showing the corresponding elemental distribution of the major metals in PM. The size and morphology of individual particles were variable (Fig. 9b–e and j) and EDX of individual particles confirmed that the PM were mainly composed of near-spherical particles of Fe, Ca, Al and Si with some fibrous Ca-rich particles. In EDX chemical maps, Na and Cl were also co-localised indicating the existence of NaCl particles (Fig. 9). Since the quartz filters are made from silica, the presence of Si in the PM was confirmed by sonicating the PM off the quartz filters onto TEM grids (SI Fig. S17). STEM-EDX of the sonicated PM showed a noticeable presence of Si in the PM which could, together with the Al, arise from aluminosilicates possibly derived from concrete building materials that line the Underground tunnels.

High-resolution SEM showed that PM fractionated during collection onto the PUF filters were highly heterogeneous in diameter and morphology (Fig. 9f–h). Individual particles with diameters of 8 μm down to 50 nm (Fig. 9f–h; indicated by arrows) were detected, with a frequent occurrence of ultrafine particles <100 nm. Some particles had a corrugated surface, possibly composed of agglomerates of ultrafine PM (Fig. 9h). A comparison between the metal composition of different size fractions ($PM_{10–2.5}$, $PM_{2.5–1}$ and $PM_{1–0.1}$), characterised by high-resolution SEM-EDX, is shown in Fig. 9i–k. Although less sensitive, this supports ICP-MS data in Table 2 that particles were composed of Fe as the major contributor and also Ca, Na, Al, K and Ti.

Next, we acquired high magnification dark-field-STEM images of PM sonicated off the filters to characterise, in detail, the chemistry and morphology of the fine and ultrafine particles. At high magnification, it became evident that some $PM_{2.5}$ and PM_1 particles were in fact agglomerates of smaller nm-sized particles with varied chemistry. STEM-EDXS maps illustrated that the $PM_{2.5}$ and PM_1 were made up of nm-sized substructures (<500 nm) composed of several different metals, including Fe, Cr, Al, and Mn (Fig. 10a, e and i). Fe and other metals were co-located with O (Fig. 10a, e and i), indicating that the Fe was most likely present in the form of various oxides. Some of the particles were mostly metal-rich (Fig. 10a), whereas other particles were composed of a cloud of carbon-rich matrix containing discrete nm-sized particles of metals (Fig. 10e and i) and the individual nm-sized particles had variable chemistries (Fig. 10b–j). High-resolution TEM of the iron-rich particles in Fig. 10i showed they were made up of <20 nm particles (Fig. 10k) constituting a larger agglomerate; high-resolution images of these (Fig. 10l) revealed lattice fringes with d-spacings characteristic of Magnetite (Ferreira et al., 2006). The characteristic planes corresponding to magnetite were labelled on the Fast Fourier transform (FFT) inset (Fig. 10l) and confirmed XRD measurements (Fig. 9a) that the most dominant iron-containing metal fraction is magnetite (Fe_3O_4), which is consistent with other studies on the underground (Smith et al., 2020). To our knowledge, this is the first time that the ultrafine fraction of London Underground Pollution PM has been characterised to be magnetite.

Fig. 9. (a). XRD pattern showing the phase chemistry of the PM, (b) ESEM image showing the morphology of the PM collected on quartz filters, and corresponding Na, Al, S, Cl, K, Ca and Fe EDX chemical maps showing the major elements detected in individual PM indicated by arrows in (b). An O map was included but was present all over the background as well as the PM. (c–e) Examples of EDXS spectra from different, representative particles (marked on maps in (b)) and their Feret diameters. (f–h) A series of high resolution secondary electron field emission gun (FEG)-SEM images showing $PM_{2.5–0.1}$ particles on a PUF filter at different magnifications. (i–k) Average atomic percentage with standard deviations of the characteristic elements including Fe, Ca, Na, Al, and K, with trace amounts of Ti, Mg, P, S and Cl detected in the PM for 3 size fractions: $PM_{2.5–10}$, $PM_{1–2.5}$ and $PM_{0.1–1}$, measured by ESEM-EDXS. n = number of particles measured.

Finally, we compared the mean atomic percent of characteristic elements in the PM for the size fractions <2.5 μm, including the ultrafine $PM_{0.1}$ fraction, using high magnification STEM-EDX (Fig. 10m–o). This technique has a higher spatial resolution than SEM and higher EDX sensitivity. The fine ($PM_{2.5–1}$ and PM_1) and ultrafine fractions ($PM_{0.1}$) all contained Fe, Na, Mg, Al, P, S, Cl, K, Ca, and also Ti, Cr, Mn, Ni transition metal ele-

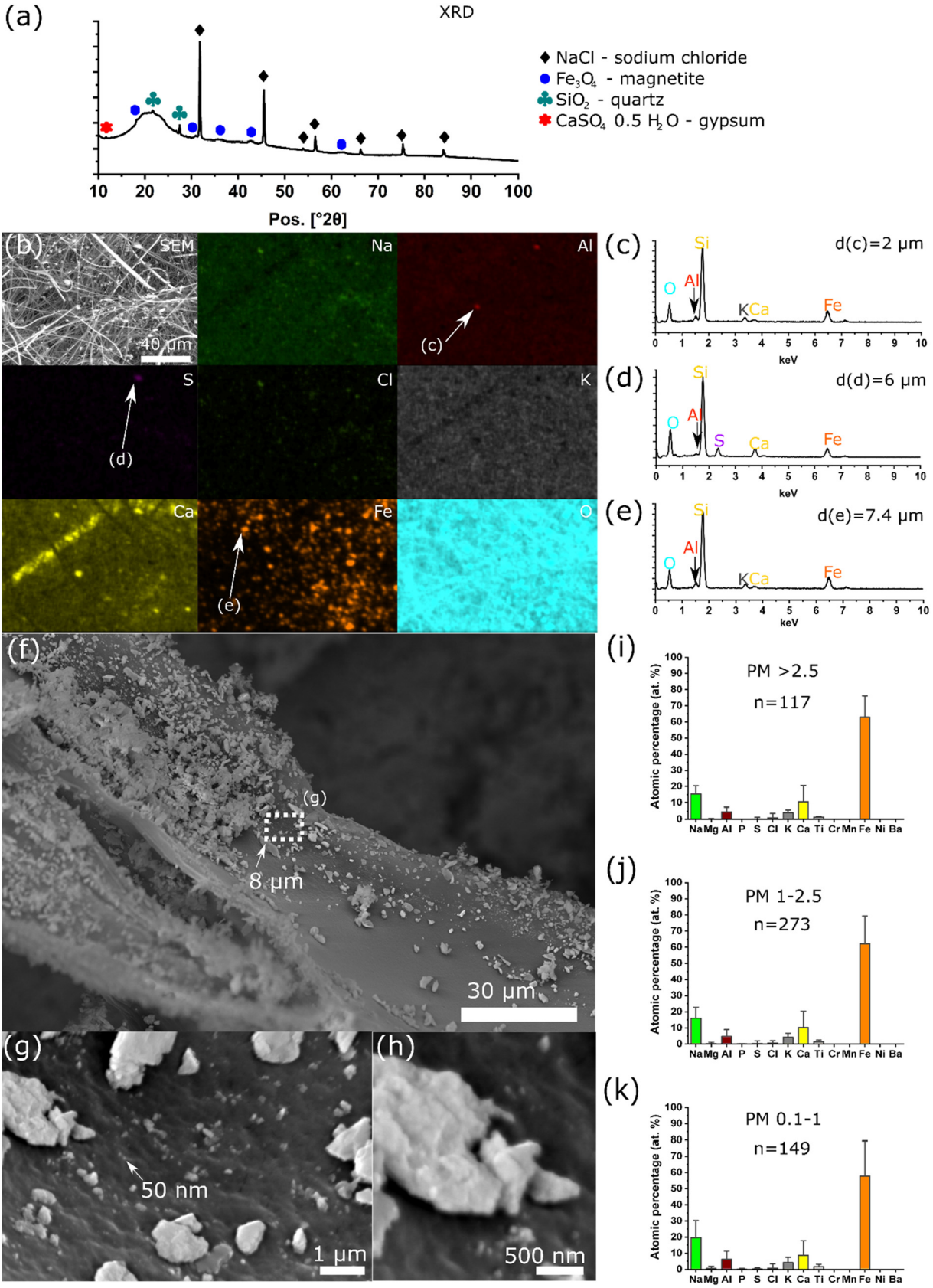

ments. Taken together, this data complements the ICP-MS analysis (Table 2) and is consistent with recent work by Smith et al. (2020), who found that $PM_{2.5}$ in the London underground contained 47 % Fe_2O_3, and 14 % metallic and mineral oxides, including CaO, but also provides fresh information about the metal-composition and internal structure and chemistry of the respirable fractions of PM: $PM_{2.5–1}$, PM_1 and $PM_{0.1}$. Notably, the $PM_{2.5}$ was made up of mixtures of metals including Fe, Cr, Zn, Al, Ni and Mn and ultrafine metal particles in a matrix of C probably derived from frictional abrasion of components of steel used in wheels and rails. The source of the carbonaceous matrix is unknown but could be from a graphitic lubricant used to reduce friction.

Aromatic hydrocarbons and PAH were detected and their concentrations are presented in Table S6. PAH are common pyrogenic products, i.e. they arise from the incomplete combustion of fossil fuels. The pyrogenic PAH are mostly present as "parent" forms, i.e. they have rings alone with no side chains.

The level of benzo(*a*)pyrene (B[*a*]P) is commonly used as a marker for carcinogenic PAHs and in the UK 0.25 ngm^{-3} B[*a*]P is recommended as an annual average air quality standard (DEFRA, 2007), an order of magnitude higher than the levels detected in our samples (Table S6). The association of PAH and inhalable PM has been described in the literature (Yan et al., 2015). Relatively high concentrations of fluoranthene and pyrene are evident in our data (Table S6). Our data are similar to measurements in the Berlin underground where fluoranthene and pyrene were found to be relatively abundant PAH (Fromme et al., 1998) and to data from the Beijing underground where the relative abundance of 4-ring PAH such as fluoranthene and pyrene was found to be higher than for surface forms of transport (Yan et al., 2015). The ratio of fluoranthene to pyrene in Berlin underground trains was found to be distinctly higher (>1.5) than observed for above-ground motor vehicles (Fromme et al., 1998) and our data also show fluoranthene to pyrene values of >1.5 for the London underground. The presence of PAH in our data suggests the circulation of partial combustion products with the underground tunnel system. The underground system is powered by electricity suggesting that the source of PAH must be from another source. Possible mechanisms for the introduction of PAH include fresh air introduced by the ventilation process or the use of oil-based lubricants within the underground system. The generation of underground transport-specific molecular distributions (i.e. relatively abundant 4-ring PAH and fluoranthene to pyrene ratios >1.5) could involve a selection or concentration process including molecular weight fractionation during atmospheric transport or, because it is recognised that PAHs are commonly associated with fine particles (Miguel et al., 2004), the preferential adsorption of certain types of PAH to particulate matter.

Collectively, these unique observations of PM chemistry are significant as these transition metal-containing ultrafine PM would be inhaled on the Underground Platform and would have the potential to drive damaging oxidation reactions in the lung, with a small fraction potentially entering the circulation (Loxham et al., 2013). Particles with a diameter of <2.5 μm can become internalised by alveolar macrophages (Hirota et al., 2013) where they have been shown to elicit pro-inflammatory responses linked to the imposition of intracellular oxidative stress (Loxham et al., 2013). Other work has shown that transition metal-containing $PM_{2.5}$ collected from an urban environment in Beijing can cause mitochondrial damage, so it is expected that the ultrafine PM collected on the London Underground could also impair the mitochondria of cells (Miao et al., 2019). This could be significant as changes to the structure and function of mitochondria can lead to human diseases including respiratory illnesses (Nunnari and Suomalainen, 2012). Other metals, including Cu and Zn, were also detected that can also contribute to cellular oxidative stress (Shen and Anastasio, 2012; Theodorou et al., 2016). Cr was measured in $PM_{2.5–0.1}$ which is of interest as this metal is known to induce cellular oxidative stress and genotoxicity (Bhabra et al., 2009; Charrier and Anastasio, 2015). These different $PM_{2.5–0.1}$ chemistries and structures will behave differently in an intracellular environment, for example, some mixtures of metals may act synergistically, to promote oxidative stress through multiple mechanisms (Charrier and Anastasio, 2015) and different particle types will degrade over different time scales, resulting in differing temporal responses. PAHs were also detected, many of which are established mutagens, carcinogens and teratogens, inducing DNA damage and oxidative stress (Patel et al., 2020). PAH has been found adsorbed on $PM_{2.5}$ (Miao et al., 2019). The most likely source of PAH is partial combustion products from vehicle exhausts (Patel et al., 2020). Yet, we have identified a PAH distribution that appears characteristic of underground transport systems (relatively abundant 4-rings and fluoranthene to pyrene ratios >1.5). The PAH weight distribution could be related to atmospheric transport or selectivity during PAH adsorption on PM.

3.6. Exposure doses

The impact on the lung to inhaled PM is a function of the PM deposition dose in different regions of HRT (Martins et al., 2015b). Therefore, we estimated the RDD for PMCs in coarse ($PM_{2.5–10}$) and fine (≤2.5 μm) particle size range and for PNCs in nucleation, accumulation and coarse particle modes for light exercise (walking) for males (Fig. 11) and females (Fig. S18). Given their higher inhalation rates and tidal volumes, the RDD is ~25 % higher for males in all size fractions than females. As an example, we discuss only the RDD of males below and the results of female RDD are presented in Fig. S18.

As expected, the total RDD of PMCs was lower during N-OpHrs than OpHrs (PM_{10} > $PM_{2.5–10}$ > $PM_{2.5}$ > PM_1: 72, 70, 79 and 77 %) (Table S7). The deposition of the fine fraction is 18 % lower than the coarse fraction. This pattern of the relative increase of coarse particle doses demonstrates the dominance of the coarse fraction in the underground train environment due to mechanical wear as a result of friction between the brake, wheel and rail track and resuspension of resulting PM (Martins et al., 2016). RDD for coarse particles was 47.04 ± 33.49 μg h^{-1} comparable to those found at urban roadsides during walking (40 to 66 μg h^{-1}; Kumar et al., 2018). The deposition rate for fine particles was 38.68 ± 22.20 μg h^{-1}, which is relatively low compared to those reported by another underground study (54.6 μg h^{-1}; Martins et al., 2015b).

The total deposition is the sum of particle depositions in three different regions of the HRT (Table S7). The ET region is the entrance to the human respiratory tract. We observed the highest deposition of coarse and fine particles compared with TB and AL regions with a contribution of 61 % and 39 %, which are ~3.3 and ~4.7 times higher during OpHrs than N-OpHrs. Particles deposited in the ET region do not then travel into the lungs. Therefore, this region acts as the first line of defence against airborne pollution (Cheng, 2003). Particles deposited here are more swiftly removed compared with those deposited in the deeper region of the lungs (Löndahl et al., 2014).

Similarly, deposition of coarse and fine particles in the TB region was ~2.7 and 4.5 times higher during OpHrs, with coarse and fine particles contributing to 46 % and 54 %, respectively. The AL region had a deposition of 19 % of coarse particles and 81 % of fine particles, which are

Fig. 10. STEM-EDXS maps of (a) $PM_{2.5}$ and (e, i) PM_1 showing co-location of transition metals within the particles and ultrafine substructures that constitute the larger particle with heterogeneous chemistries. (a) DF-STEM image of a representative 2.5 μm particle and corresponding chemical maps of C, O, Na, Al, Si, S, Cl, Ca, Cr, Mn and Fe (b, c, d) EDXS spectra of selected substructures with their respective Feret diameters. (e) DF-STEM image of a representative <1 μm particle and corresponding chemical maps of C, O, Na, Al, Si, S, Cl, Ca, Cr, Mn and Fe (f, g, h) EDXS spectra of selected substructures with their respective Feret diameters. (i) DF-STEM image of a representative Fe-rich 1 μm particle and corresponding chemical maps showing C, O, Na, Al, Si, S, Cl, Ca, Cr, Mn and Fe. (j) EDXS spectra of selected nm-substructures with their respective Feret diameters. (k) TEM image of iron-containing particle (seen on (i)). (l) High-resolution image of particles seen in (k) and corresponding FFT pattern of the selected region showing space frequencies of planes characteristic of magnetite (111–2.07 nm^{-1}; 311–3.9 nm^{-1}; 400–4.7 nm^{-1}). (m–o) Average atomic percentage of the PM for three size fractions of $PM_{0.1}$, $PM_{0.1–1}$ and $PM_{1–2.5}$ measured using STEM-EDXS.

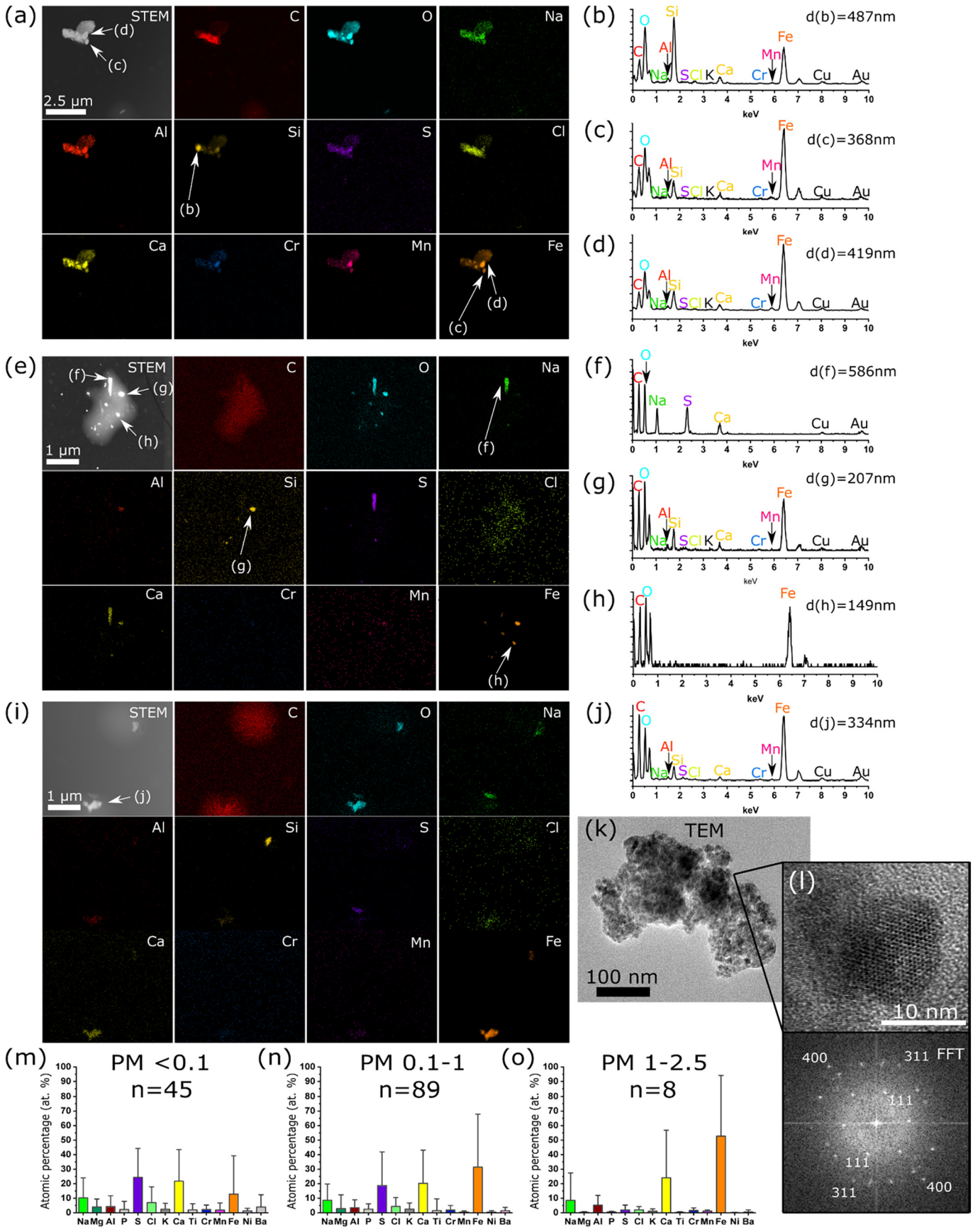
(a)
STEM
(d)
(c)
2.5 μm
C
O
Na
Al
Si
(b)
S
Cl
Ca
Cr
Mn
Fe
(d)
(c)
(b)
d(b)=487nm
d(c)=368nm
d(d)=419nm
keV
(e)
(f)
(g)
(h)
1 μm
(f)
(g)
(h)
d(f)=586nm
d(g)=207nm
d(h)=149nm
(i)
(j)
d(j)=334nm
(k)
TEM
100 nm
(l)
10 nm
400
311
FFT
111
111
311
400
(m)
PM <0.1
n=45
(n)
PM 0.1-1
n=89
(o)
PM 1-2.5
n=8
Atomic percentage (at. %)
Na Mg Al P S Cl K Ca Ti Cr Mn Fe Ni Ba

Table 2
$PM_{2.5–0.1}$, $PM_{10–2.5}$ and PM_{10} chemical composition measured by ICP-MS as a proportion of the weight of each pollution fraction collected.

Component	03 Oct 2020 - weekend (mg/g pollution)			15 Oct 2020 - weekday (mg/g pollution)		
	$PM_{2.5–0.1}$	$PM_{10–2.5}$	PM_{10}	$PM_{2.5–0.1}$	$PM_{10–2.5}$	PM_{10}
Na	6.559	5.997	13.021	6.835	7.941	8.030
Mg	1.743	1.863	4.029	2.204	2.853	2.277
Al	4.125	3.769	20.697	5.563	3.726	10.047
P	0.839	0.876	5.577	1.262	1.154	2.752
K	5.564	5.488	15.683	7.683	6.894	7.738
Ca	23.855	32.623	92.994	29.229	47.347	44.761
Ti	0.140	0.203	1.155	0.193	0.214	0.549
V	0.015	0.014	0.066	0.022	0.015	0.035
Cr	0.456	0.305	0.401	0.606	0.302	0.221
Mn	1.967	1.386	2.224	2.684	1.405	1.264
Fe	592.944	592.250	399.525	746.088	758.061	227.331
Co	0.016	0.015	0.031	0.023	0.015	0.017
Ni	0.154	0.144	0.291	0.210	0.142	0.159
Cu	0.331	0.244	0.522	0.465	0.249	0.301
Zn	0.292	0.222	0.627	0.408	0.218	0.352
Sr	0.031	0.047	0.192	0.042	0.053	0.095
Mo	0.372	0.330	0.231	0.335	0.288	0.121
Cd	0.001	0.001	0.002	0.002	0.001	0.001
Sb	0.010	0.010	0.014	0.017	0.013	0.008
Ba	0.081	0.069	0.288	0.128	0.095	0.177
Pb	0.023	0.031	0.101	0.051	0.040	0.054

~1.2 and ~4.7 times higher during OpHrs compared with N-OpHrs. The percentage deposition of fine fractions increased gradually compared with the coarse fraction in the TB and AL regions, supporting the assumption that the finer the particles, the deeper they can penetrate the respiratory system (Sturm, 2016). Similar trends were observed for the fine particle deposition in the different regions of HRT in a study of a subway system in Barcelona with a higher deposition of fine particles in the AL region (11.5 %) compared to the TB (3.9 %) region (Martins et al., 2015b). The RDD rates of PNCs showed higher deposition in nucleation mode, followed by accumulation and coarse modes, during OpHrs. This trend is expected as the PNCs are dominated by nucleation mode (69 % of total PNCs), followed by accumulation (27 %) mode and a modest fraction in the coarse mode (4 %) (Fig. 5). The deposition of nucleation, accumulation and coarse mode particles was 17, 60 and 72 % lower during N-OpHrs compared with OpHrs. Nucleation mode particles are usually formed as a result of the gas to particle conversion process (Kumar et al., 2011, 2014). However, there are no direct sources of gaseous emissions in the underground to support the formation of nucleation mode particles and thus explaining the modest differences observed between the OpHrs and N-OpHrs. Metallic brake abrasions at stations have been reported to produce particles down to 20 nm (Namgung et al., 2016; Grigoratos and Martini, 2015; Kukutschová et al., 2011), which would have contributed to the increased differences for accumulation and coarse mode particles during OpHrs due to train activity compared with N-OpHrs.

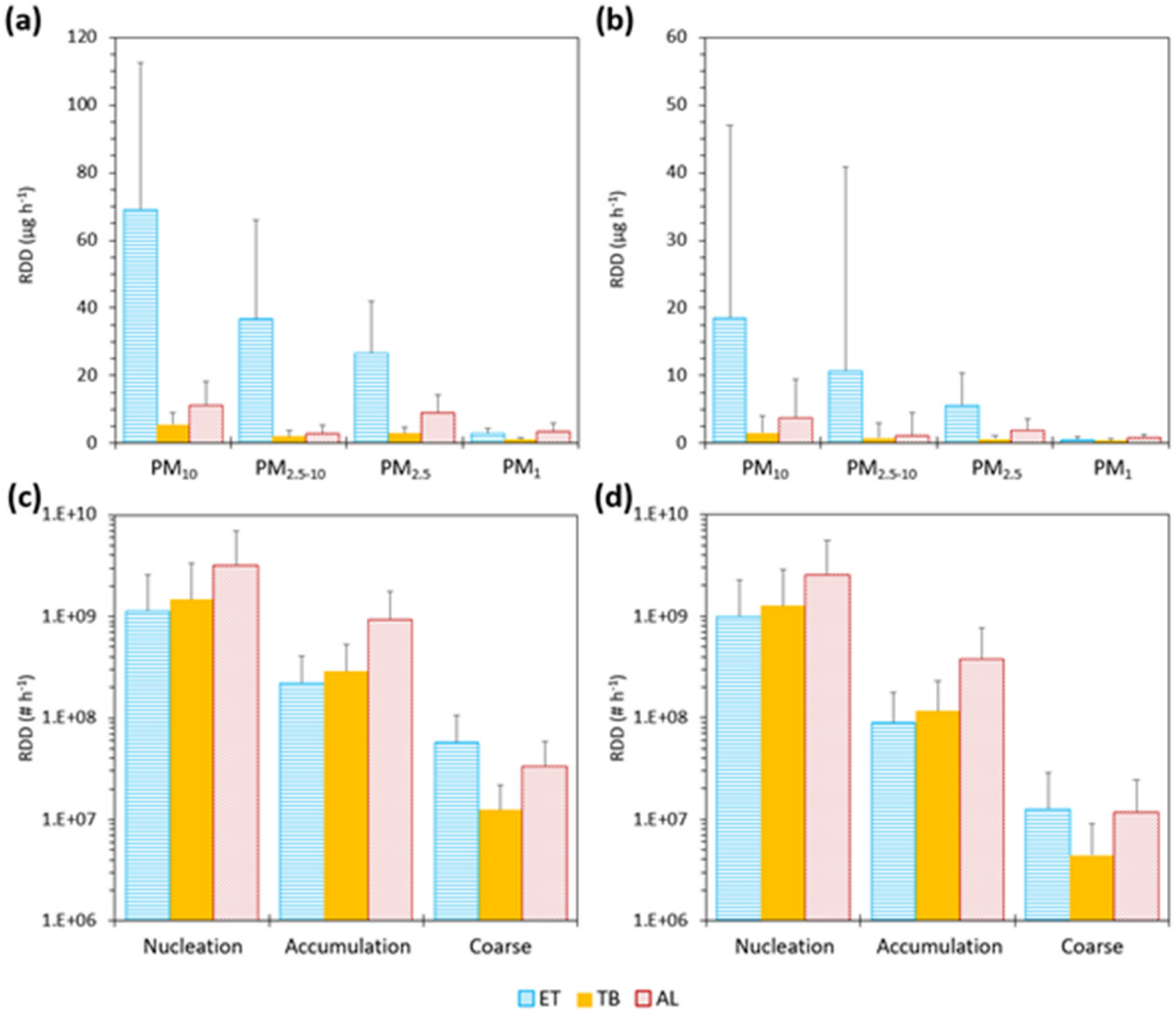

Fig. 11. Respiratory deposition doses for males of various particle sizes of PM and PNCs in the underground during OpHrs (05:00–00:00) and N-OpHrs (00:00–05:00) for (a) RDD of PMCs during OpHrs; (b) RDD of PMCs during N-OpHrs; (c) RDD of PNCs during OpHrs; (d) RDD of PNCs during N-OpHrs. ET, TB and AL refer to the extrathoracic region, tracheobronchial region and alveolar region of the human respiratory tract.

Deposition is a function of the number of particles in a particular mode and, as nucleation mode particles had the highest PNCs (Fig. 5), their deposition was highest in all three regions (ET, TB and AL), followed by the deposition of accumulation and coarse mode particles (Fig. 11). In the ET region, the deposition of nucleation mode particles during OpHrs was $1.12 \pm 1.45 \times 10^9\ h^{-1}$, 80 % and 95 % higher than those in accumulation and coarse modes, respectively. In the TB region, the deposition of nucleation mode particles during OpHrs was $1.47 \pm 1.85 \times 10^9\ h^{-1}$, 80 % and 99 % higher than those in accumulation and coarse modes, respectively. Finally, in the AL region, the deposition of nucleation mode particles during OpHrs was $3.18 \pm 3.72 \times 10^9\ h^{-1}$, 70 % and 99 % higher than those in accumulation and coarse modes, respectively. N-OpHrs followed the same trend. The nucleation and accumulation mode particles followed the same pattern of deposition (AL > TB > ET) in contrast to the coarse mode (ET > AL > TB; Fig. 11). These observations are consistent with the expectation that coarse particles are deposited largely in the upper HRT region.

4. Conclusions

The following conclusions are drawn from the extensive monitoring and physicochemical analysis of the PM in different size fractions:

- Variation in mass concentration of PM and BC aerosols correlated with train and passenger numbers, peaking at busy times. Airborne pollutant concentrations decreased in N-OpHrs, highlighting the aerosol settling process. In contrast during OpHrs, 64 % of PNCs were found in nucleation mode which increased during N-OpHrs; these could be related to the entrainment of surface air into the underground station. PNDs were similar between 6 and 15 nm during both OpHr and NOpHr, but only larger particles decreased during N-OpHrs. Point biserial correlation analysis indicates that trains arriving at the underground station caused some PM concentration variation, however, PNC were found to be weakly correlated with train movement.
- Poor ventilation on the underground platform with a replenishment of fresh air of 0.24 ± 0.11 times per hour could be responsible for the accumulation of pollutants in the Underground system over time.
- The mean RDD of PMCs for coarse particles was ~1.2 times higher than fine particles, showing the dominance of coarse particle generation in the underground subway system. The deposition was higher during OpHrs than N-OpHrs.
- The mass of fine particles deposited in the alveolar region was 81 % higher than coarse particles. Similarly, the RDD of PNCs showed higher deposition of coarse mode particles, followed by accumulation and nucleation mode during OpHrs. The AL region had a higher deposition of nucleation and accumulation mode particles during OpHrs and N-OpHrs. This data highlights that coarser particles mainly deposit in the upper HRT regions, whereas the ultrafine particles can reach the deeper region of lungs.
- PM of all size distributions are largely composed of Fe in the form of magnetite and trace contributions of other metals including Cr, Al, Ni and Mn which could potentially cause cellular toxicity. The ultrafine fraction of PM was composed of transition metals including Fe with contributions of Cr, Al, Ni and Mn and made up of <20 nm particles of Magnetite. The fine PM2.5 and PM1 particles were hybrids of nm-sized structures of metal-mixtures in a larger matrix of metal or carbon that could affect their degradation behaviour inside cells.

To our knowledge, this is the first study that describes the composition and structure of the ultrafine and fine fractions of pollution PM. It is focussed on one Underground station with measurements performed over a limited time period, however the measurements of diurnal variations in PM and BC mass and PM composition (excluding the ultrafine fraction) are consistent with existing studies on different underground systems (Section 3.3) and are most probably applicable to other underground systems depending on different factors such as the age of the line, trains in use, construction technique, passenger density and station depth (Hester and Harrison, 2009). Although commuter exposure time on platforms is generally limited to an average of around 2 to 5 min (Martins et al., 2015a), and there is a dominance of coarse particles, the continuous exposure to the increased deposition doses of fine and ultrafine PM composed of iron oxides and other toxic metals and PAHs in the AL region for a prolonged period in underground train systems, could lead to increased cellular toxicity and detrimental health effects (Sturm, 2016). For example, these nanometer-sized particles could become internalised by cells, amplifying toxicity or further penetrate the lung barriers crossing into the bloodstream contributing to adverse cardiovascular and respiratory responses (Patel et al., 2020; Karlsson et al., 2005; Patel et al., 2020). In addition to previous observations and recommendations made regarding the cumulative risk to the health of workers or commuters (Seaton et al., 2005), we would like to add the following points:

- The possible adverse health effects associated with exposure to the specific underground aerosols that we have described and particularly the potentially toxic metals identified here in the finer fractions needs further investigation. In particular, we need to understand whether these particles are more toxic than those present on the busy London roadside.
- Future research should focus on the real-time-spatial distribution of PM and ventilation efficacy through a better understanding of local air flows and pollutant dispersion characteristics, identifying locations with very high levels of PM in the underground. These evidence-based approaches can help transport providers to develop and establish strategies to mitigate the impact of PM on passenger health.
- We recognise that London Underground has a cleaning programme to remove particulate matter but that this is a complex and slow task. We recommend that improved ventilation is also needed to disperse and remove the high levels of PM observed during operating hours and use of screen doors between the train and platform such as on the new Elizabeth Line. Given that the underground environments are complex in terms of their built structure and the dynamic flow of the people, more sophisticated modelling approaches are also needed to estimate their ventilation in real-time.
- Vulnerable passengers might consider how they can limit their exposure to particulate matter while travelling in the underground. This could include avoiding rush hours where possible and/or wearing facemasks capable of filtering out ultrafine particles.
- The UK's Health and Safety Executive for example may consider if it is necessary to establish separate Workplace Exposure Limit categories for smaller PM fractions than the currently measured larger-sized fraction, with lower limits given their potential toxicity and capacity to cross the lung barrier. In the meanwhile, local authorities should consider collecting similar detailed data (particularly on the smaller PM fractions) on public transport to develop evidence-based, localised strategies to reduce passenger exposure to air pollution.

CRediT authorship contribution statement

Prashant Kumar: Conceptualization, Funding acquisition, Methodology, Formal Analysis, Project administration, Resources, Supervision, Visualization, Writing - Original Draft, Writing - review and editing; **Juan C. Zavala-Reyes**: Data curation, Formal Analysis, Writing - original draft, Investigation, Validation, Writing - review and editing; **Gopinath Kalaiarasan**: Data collection, Writing - review and editing; **Hisham Abubakar-Waziri**: Writing - review and editing; **Gloria Young**: Investigation, Writing - Original Draft, Writing - review and editing; **Ian Mudway**: Writing - review and editing; **Claire Dilliway**: Writing - review and editing; **Ramzi Lakhdar**: Writing - review and editing; **Sharon Mumby**: Writing - review and editing; **Michał M. Kłosowski**: Writing - review and editing; **Christopher C. Pain**: Funding acquisition, Writing - review and editing; **Ian M Adcock**: Writing - review and editing; **Jonathan S Watson**: Writing - review and editing; **Mark A. Sephton**: Writing - review and editing; **Kian Fan**

Chung: Funding acquisition, Writing - review and editing; **Alexandra E Porter**: Investigation, Writing - Original Draft, Writing - review and editing.

Data availability

Data will be made available on request.

Declaration of competing interest

The authors declare that they have no known competing financial interests or personal relationships that could have appeared to influence the work reported in this paper.

Acknowledgements

This work is supported by the EPSRC-funded project INHALE (Health assessment across biological length scales for personal pollution exposure and its mitigation; Grant No. EP/T003189/1). The authors thank the INHALE Programme Manager, Claire Dilliway, for her help in facilitating the access to the sites and the INHALE project team from Imperial College London and University of Edinburgh for valuable discussions. We would also like to thank Hugh Corrigan (Building Manager District Line), Philip Flint (SHE Business Partner), Lilian Luke (Customer Service Manager South Kensington), Abdul Rahim (Area Manager South Kensington) and Nick Wilson (Occupational Hygiene Manager) from Transport for London for helpful discussions and arranging permissions for access to carry out fieldwork on the underground station. The authors also thank GCARE team members Mamatha Tomson, Sarkawt Hama and Arvind Tiwari for their help during the fieldwork. We are grateful to Imperial College London Estates for their financial support to the INHALE project fieldwork and, in particular, Luqman Jalloh (Electrical Design Engineer) from Imperial College London for his assistance in arranging logistical support for the fieldwork. We thank Electrical technicians from Elecro Ltd.; Sean Burke, Dan Sim and Gary Glyde, for providing assistance during field measurements. The authors thank Dr. Rebekah Moore and Dr. Alex Griffiths at the London Metallomics Facility, funded by the Wellcome Trust (grant reference 202902/Z/16/Z), for ICP-MS measurements. We thank Marta Chiapasco and Richard Sweeney for acquiring the XRD spectra. IM is part funded by the NIHR Health Protection Research Unit in Environmental Exposures and Health, a partnership between UKHSA and Imperial College London. The views expressed are those of the author(s) and not necessarily those of the NIHR, UKHSA, the Department of Health and Social Care, or the EPSRC.

Appendix A. Supplementary data

Supplementary data to this article can be found online at https://doi.org/10.1016/j.scitotenv.2022.159315.

References

Aarnio, P., Yli-Tuomi, T., Kousa, A., Mäkelä, T., Hirsikko, A., Hämeri, K., Räisänen, M., Hillamo, R., Koskentalo, T., Jantunen, M., 2005. The concentrations and composition of and exposure to fine particles ($PM_{2.5}$) in the Helsinki subway system. Atmos. Environ. 39, 5059–5066.

Abhijith, K.V., Kumar, P., 2019. Field investigations for evaluating green infrastructure effects on air quality in open-road conditions. Atmos. Environ. 201, 132–147.

Abhijith, K.V., Kumar, P., 2021. Evaluation of respiratory deposition doses in the presence of green infrastructure. Air Qual. Atmos. Health 14, 911–924.

Ariëns, J.P.E., Joosten, T.A., Schriemer, W., 2008. Guidebook Sports Accommodations (In Dutch). Handboek Sport Accommodaties. ISA Sport.

ASHRAE, 2013. Ventilation for Acceptable Indoor Air Quality. American Society of Heating, Refrigerating and Air-Conditioning Engineers.

Azarmi, F., Kumar, P., Mulheron, M., 2014. The exposure to coarse, fine and ultrafine particle emissions from concrete mixing, drilling and cutting activities. J. Hazard. Mater. 279, 268–279.

Beheshti, A., Egle, C., David, J.S., Sylvain, V.C., 2018. Global transcriptomic analysis suggests carbon dioxide as an environmental stressor in spaceflight: a systems biology GeneLab case study. Sci. Rep. 8, 1–10.

Bhabra, G., Sood, A., Fisher, B., Cartwright, L., Saunders, M., Evans, W.H., Surprenant, A., Lopez-Castejon, G., Mann, S., Davis, S.A., Hails, L.A., Ingham, E., Verkade, P., Lane, J., Heesom, K., Newson, R., Case, C.P., 2009. Nanoparticles can cause DNA damage across a cellular barrier. Nat. Nanotechnol. 4, 876–883.

Bhadeshia, H.K.D.H., 2002. In: Buschow, K., Cahn, R.W., Flemings, M.C., Iischner, B., Kramer, E.J., Mahajan, S. (Eds.), Encyclopedia of Materials Science: Science and Technology. Pergamon Press, Elsevier Science, pp. 1–7 ISBN 0-08-0431526.

Canha, N., Mandin, C., Ramalho, O., Wyart, G., Ribéron, J., Dassonville, C., Hänninen, O., Almeida, S.M., Derbez, M., 2016. Assessment of ventilation and indoor air pollutants in nursery and elementary schools in France. Indoor Air 26, 350–365.

Carslaw, D.C., Ropkins, K., 2012. openair — An R package for air quality data analysis. Environ. Model. Softw. 27-28, 52–61.

Cartenì, A., Cascetta, F., Henke, I., Molitierno, C., 2020. The role of particle resuspension within PM concentrations in underground subway systems. Int. J. Environ. Sci. Technol. 17, 4075–4094.

Charles, K.E., Reardon, J.T., Robert, J.M., 2005. Indoor Air Quality and Thermal Comfort in Open-Plan Offices. 64. Institute for Research in Construction, National Research Council of Canada, pp. 1–6.

Charrier, J.G., Anastasio, C., 2015. Rates of hydroxyl radical production from transition metals and quinones in a surrogate in a surrogate lung fluid. Environ. Sci. Technol. 49 (15), 9317–9325.

Chen, T., Cao, S.J., Wang, J., Nizamani, A.G., Feng, Z., Kumar, P., 2021. Influences of the optimized air curtain at subway entrance to reduce the ingress of outdoor airborne particles. Energy Build. 244, 111028.

Cheng, Yung Sung, 2003. Aerosol deposition in the extrathoracic region. Aerosol Sci.Technol. 37, 659–671.

Cheng, Y.H., Liu, Z.S., Yan, J.W., 2012. Comparisons of PM_{10}, $PM_{2.5}$, particle number, and CO_2 levels inside metro trains traveling in underground tunnels and on elevated tracks. Aerosol Air Qual. Res. 12, 879–891.

COMEAP, 2018. Statement on the evidence for health effects in the travelling public associated with exposure to particulate matter in the London Underground.Available at:Committee on the Medical Effects of Air Pollutants (accessed 18 December 2019) https://assets.publishing.service.gov.uk/government/uploads/system/uploads/attachment_data/file/769884/COMEAP_TfL_Statement.pdf.

Cusack, M., Talbot, N., Ondráček, J., Minguillón, M.C., Martins, V., Klouda, K., Schwarz, J., Ždímala, V., 2015. Variability of aerosols and chemical composition of PM_{10}, $PM_{2.5}$ and PM_1 on a platform of the Prague underground metro. Atmos. Environ. 118, 176–183.

DEFRA, 2007. The Air Quality Strategy for England, Scotland, Wales and Northern Ireland. Available at https://assets.publishing.service.gov.uk/government/uploads/system/uploads/attachment_data/file/69336/pb12654-air-quality-strategy-vol1-070712.pdf. (Accessed 31 October 2021).

DEFRA, 2021. Particulate matter (PM10) concentrations in the UK, 1992 to 2021. Available at https://www.gov.uk/government/statistical-data-sets/env02-air-quality-statistics. (Accessed 29 April 2022).

DfT, 2021. Transport Use during the Coronavirus (COVID-19) Pandemic. Available at https://www.gov.uk/government/statistics/transport-use-during-the-coronavirus-covid-19-pandemic. (Accessed 6 January 2021).

Ferreira, F.F., Granado, E., Carvalho Jr, W., Kycia, S.W., Bruno, D., Droppa Jr, R., 2006. X-ray powder diffraction beamline at D10B of LNLS: application to the Ba_2FeReO_6 double perovskite. J. Synchrotron Radiat. 13, 46–53.

Fromme, H., Oddoy, A., Piloty, M., Krause, M., Lahrz, T., 1998. Polycyclic aromatic hydrocarbons (PAH) and diesel engine emission (elemental carbon) inside a car and a subway train. Sci. Total Environ. 217, 165–173.

Gilardoni, S., Vignati, E., Wilson, J., 2011. Using measurements for evaluation of black carbon modeling. Atmos. Chem. Phys. 11, 439–455.

Grana, M., Toschi, N., Vicentini, L., Pietroiusti, A., Magrini, A., 2017. Exposure to ultrafine particles in different transport modes in the city of Rome. Environ. Pollut. 228, 201–210.

Griebel, Stefanie, Webb, Molly M., Campanella, Osvaldo H., Craig, Bruce A., Weil, Clifford F., Tuinstra, Mitchell R., 2019. The alkali spreading phenotype in sorghum bicolor and its relationship to starch gelatinization. J. Cereal Sci. 86, 41–47.

Grigoratos, T., Martini, G., 2015. Brake wear particle emissions: a review. Environ. Sci. Pollut. Res. 22, 2491–2504.

Guo, L., Hu, Y., Hu, Q., Lin, J., Li, C., Chen, J., Li, L., Fu, H., 2014. Characteristics and chemical compositions of particulate matter collected at the selected metro stations of Shanghai, China. Sci. Total Environ. 496, 443–452.

Hagler, G.S.W., Yelverton, T.L.B., Vedantham, R., Hansen, A.D.A., Turner, J.R., 2011. Post-processing method to reduce noise while preserving high time resolution in aethalometer real-time black Carbon Data. Aerosol Air Qual. Res. 11, 539–546.

Hamdan, N.M., Alawadhi, H., 2020. X-ray diffraction as a major tool for the analysis of $PM_{2.5}$ and PM_{10} aerosols. Powder Diffract. 35, 98–103.

Hänninen, O., 2013. Novel second-degree solution to single zone mass-balance equation improves the use of build-up data in estimating ventilation rates in classrooms. J.Chem. Health Saf. 20, 14–19.

Harrison, R.M., Jones, A.M., Gietl, J., Yin, J., Green, D.C., 2012. Estimation of the contributions of brake dust, tire wear, and resuspension to non-exhaust traffic particles derived from atmospheric measurements. Environ.Sci.Technol. 46, 6523–6529.

Hester, R.E., Harrison, R.M., 2009. Air Quality in Urban Environments. Royal Society of Chemistry, Cambridge 978-1-84755-907-4.

Hinds, W.C., 1999. Aerosol Technology: Properties, Behaviour and Measurement of Airborne Particles. John Wiley & Sons, London.

Hirota, K., Kawamoto, T., Nakajima, T., Makino, K., Terada, H., 2013. Distribution and deposition of respirable PLGA microspheres in lung alveoli. Colloids Surf. B. 1, 92–97.

Hofmann, W., 2011. Modelling inhaled particle deposition in the human lung-a review. J. Aerosol Sci. 42, 693–724.

ICRP, 1994. Human respiratory tract model for radiological protection. ICRP Publication 66. Ann. ICRP 24 (1-3).

Järnström, H., Saarela, K., Kalliokoski, P., Pasanen, A.-L., 2006. Reference values for indoor air pollutant concentrations in new residential buildings in Finland. Atmos. Environ. 40, 7178–7191.

Joodatnia, P., Kumar, P., Robins, A., 2013. The behaviour of traffic produced nanoparticles in a car cabin and resulting exposure rates. Atmos. Environ. 65, 40–51.

Kam, W., Cheung, K., Daher, N., Sioutas, C., 2011a. Particulate matter (PM) concentrations in underground and ground-level rail systems of the Los Angeles Metro. Atmos. Environ. 45, 1506–1516.

Kam, W., Ning, Z., Shafer, M.M., Schauer, J.J., Sioutas, C., 2011b. Chemical characterization and redox potential of coarse and fine particulate matter (PM) in underground and ground-level rail systems of the Los Angeles metro. Environ. Sci. Technol. 45, 6769–6776.

Karlsson, H.L., Nilsson, L., Moller, L., 2005. Subway particles are more genotoxic than street particles and induce oxidative stress in cultured human lung cells. Chem. Res. Toxicol. 18, 19–23.

Keast, L., Bramwell, L., Maji, K.J., Rankin, J., Namdeo, A., 2022. Air quality outside schools in Newcastle upon Tyne, UK: an investigation into NO_2 and PM concentrations and PM respiratory deposition. Atmosphere 13 (2), 1–16.

Kukutschová, J., Moravec, P., Tomásek, V., Matejka, V., Smolík, J., Schwarz, J., Seidlerová, J., Safárová, K., Filip, P., 2011. On airborne nano/micro-sized wear particles released from low-metallic automotive brakes. Environ. Pollut. 159, 998–1006.

Kumar, P., Goel, A., 2016. Concentration dynamics of coarse and fine particulate matter at and around signalised traffic intersections. Environ. Sci.: Process. Impacts 18, 1220–1235.

Kumar, P., Ketzel, M., Vardoulakis, S., Pirjola, L., Britter, R., 2011. Dynamics and dispersion modelling of nanoparticles from road traffic in the urban atmospheric environment - a review. J. Aerosol Sci. 42, 580–603.

Kumar, P., Morawska, L., Birmili, W., Paasonen, P., Hu, M., Kulmala, M., Harrison, R.M., Norford, L., Britter, R., 2014. Ultrafine particles in cities. Environ. Int. 66, 1–10.

Kumar, P., Rivas, I., Singh, A.P., Ganesh, V.J., Ananya, M., Frey, H.C., 2018. Dynamics of coarse and fine particle exposure in transport microenvironments. Clim. Atmos. Sci. 11, 1–12.

Kumar, P., Kalaiarasan, G., Porter, A.E., Pinna, A., Kłosowski, M.M., Demokritou, P., Chung, K.F., Pain, C., Arvind, D.K., Arcucci, R., Adcock, I.M., Dilliway, C., 2021. An overview of methods of fine and ultrafine particle collection for physicochemical characterisation and toxicity assessments. Sci. Total Environ. 756, 143553.

Lima, B.D., Teixeira, E.C., Hower, J.C., Civeira, M.S., Ramírez, O., Yang, C.X., Oliveira, M.L.S., Silva, L.F.O., 2021. Metal-enriched nanoparticles and black carbon: a perspective from the Brazil railway system air pollution. Geosci. Front. 12.

Löndahl, J., Möller, W., Pagels, J.H., Kreyling, W.G., Swietlicki, E., Schmid, O., 2014. Measurement techniques for respiratory tract deposition of airborne nanoparticles: a critical review. J. Aerosol Med. Pulm. Drug Deliv. 27, 229–254.

Loxham, M., Nieuwenhuijsen, M.J., 2019. Health effects of particulate matter air pollution in underground railway systems- a critical review of the evidence. Part. Fibre Toxicol. 16, 1–24.

Loxham, M., Cooper, M.J., Gerlofs-Nijland, M.E., Cassee, F.R., 2013. Physicochemical characterization of airborne particulate matter at a mainline underground railway station. Environ. Sci. Technol. 47, 3614–3622.

LTM, 2022. Transport stories. Available atLondon Transport Museum. https://www.ltmuseum.co.uk. (Accessed 31 August 2022).

Martins, V., Moreno, T., Minguillón, M.C., Amato, F., de Miguel, E., Capdevila, M., Querol, X., 2015a. Exposure to airborne particulate matter in the subway system. Sci. Total Environ. 511, 711–722.

Martins, V., Cruz Minguillón, M., Moreno, T., Querol, X., de Miguel, E., Capdevila, M., Centelles, S., Lazaridis, M., 2015b. Deposition of aerosol particles from a subway microenvironment in the human respiratory tract. J. Aerosol Sci. 90, 103–113.

Martins, V., Moreno, T., Mendes, L., Eleftheriadis, K., Diapouli, E., Alves, C.A., Duarte, M., de Miguel, E., Capdevila, M., Querol, X., Minguillón, M.C., 2016. Factors controlling air quality in different European subway systems. Environ. Res. 146, 35–46.

Martins, V., Correia, C., Cunha-Lopes, I., Faria, T., Diapouli, E., Manousakas, M.I., Eleftheriadis, K., Almeida, S.M., 2021. Chemical characterisation of particulate matter in urban transport modes. J. Environ. Sci. 100, 51–61.

Martrette, J.M., Egloff, C., Clément, C., Yasukawa, K., Thornton, S.N., Trabalon, M., 2017. Effects of prolonged exposure to CO_2 on behaviour, hormone secretion and respiratory muscles in young female rats. Physiol. Behav. 177, 257–262.

Mendes, L., Gini, M.I., Biskos, G., Colbeck, I., Eleftheriadis, K., 2018. Airborne ultrafine particles in a naturally ventilated metro station: dominant sources and mixing state determined by particle size distribution and volatility measurements. Environ. Pollut. 239, 82–94.

Miao, X., Li, W., Niu, B., Li, J., Sun, J., Qin, M., Zhou, Z., 2019. Mitochondrial dysfunction in endothelial cells induced by airborne fine particulate matter (<2.5μm). J. Appl. Toxicol. 39, 1424–1432.

Miguel, A.H., Eiguren-Fernandez, A., Jaques, P.A., Froines, J.R., Grant, B.L., Mayo, P.R., Sioutas, C., 2004. Seasonal variation of the particle size distribution of polycyclic aromatic hydrocarbons and of major aerosol species in Claremont, California. Atmos. Environ. 38, 3241–3251.

Minguillón, M.C., Reche, C., Martins, V., Amato, F., de Miguel, E., Capdevila, M., Centelles, S., Querol, X., Moreno, T., 2018. Aerosol sources in subway environments. Environ. Res. 167, 314–328.

Mohsen, M., Ahmed, M.B., Zhou, J.L., 2018. Particulate matter concentrations and heavy metal contamination levels in the railway transport system of Sydney, Australia. Transp. Res. Part D: Transp. Environ. 62, 112–124.

Moreno, T., Reche, C., Rivas, I., Minguillón, M.C., Martins, V., Vargas, C., Buonanno, G., Parga, J., Pandolfi, M., Brines, M., Ealo, M., Fonseca, A.S., Amato, F., Sosa, G., Capdevila, M., Miguel, E., Querol, X., Gibbons, W., 2015. Urban air quality comparison for bus, tram, subway and pedestrian commutes in Barcelona. Environ. Res. 142, 495–510.

Moreno, T., Martins, V., Querol, X., Jones, T., BéruBé, K., Minguillón, M.C., Amato, F., Capdevila, M., de Miguel, E., Centelles, S., Gibbons, W., 2015b. A new look at inhalable metalliferous airborne particles on rail subway platforms. Sci. Total Environ. 505, 367–375.

Mugica-Álvarez, V., Figueroa-Lara, J., Romero-Romo, M., Sepúlvea-Sánchez, J., López-Moreno, T., 2012. Concentrations and properties of airborne particles in the Mexico City subway system. Atmos. Environ. 49, 284–293.

Namgung, H.G., Kim, J.B., Woo, S.H., Park, S., Kim, M., Kim, M.S., Bae, G.M., Park, D., Kwon, S.B., 2016. Generation of nanoparticles from friction between railway brake disks and pads. Environ.Sci.Technol. 50, 3453–3461.

NOAA, 2021. Trends in Atmospheric Carbon Dioxide. Available at https://gml.noaa.gov/ccgg/trends/. (Accessed 15 June 2020).

Nunnari, J., Suomalainen, A., 2012. Mitochondria: in sickness and in health. Cell 148, 1145–1159.

Olesen, B.W., Parsons, K.C., 2002. Introduction to thermal comfort standards and to the proposed new version of EN ISO 7730. Energy Build. 34, 537–548.

Pan, S., Du, S., Wang, X., Zhang, X., Xia, L., Liu, J., Pei, F., Wei, Y., 2019. Analysis and interpretation of the particulate matter (PM_{10} and $PM_{2.5}$) concentrations at the subway stations in Beijing,China. Sustain. Cities Soc. 45, 366–377.

Patel, A.B., Shaikh, S., Jain, K.R., Desai, C., Madamwar, D., 2020. Polycyclic aromatic hydrocarbons: sources, toxicity, and remediation approaches. Front. Microbiol. 11, 2675.

Perrino, C., Marcovecchio, F., Tofful, L., Canepari, S., 2015. Particulate matter concentration and chemical composition in the metro system of Rome, Italy. Environ. Sci. Pollut. Res. 22, 9204–9214.

Python Core Team, 2018. Python: a dynamic, open source programming language. Available fromPython Softw. Found. https://www.python.org/.

Querol, X., Moreno, T., Karanasiou, A., Reche, C., Alastuey, A., Viana, M., Font, O., Gil, J., De Miguel, E., Capdevila, M., 2012. Variability of levels and composition of PM_{10} and $PM_{2.5}$ in the Barcelona metro system. Atmos. Chem. Phys. 12, 5055–5076.

R Core Team, 2020. R: A Language and Environment for Statistical Computing.Available fromR Foundation for Statistical Computing, Vienna, Austria (accessed 08.05.2022) http://www.R-project.org/.

Ramalho, O., Mandin, C., Ribéron, J., Wyart, G., 2013. Air stuffiness and air exchange rate in French schools and day-care centres. Int. J. Vent. 12, 175–180.

Raut, J.C., Chazette, P., Fortain, A., 2009. Link between aerosol optical, microphysical and chemical measurements in an underground railway station in Paris. Atmos. Environ. 43, 860–868.

Rivas, I., Kumar, P., Hagen-Zanker, A., 2017a. Exposure to air pollutants during commuting in London: are there inequalities among different socio-economic groups? Environ. Int. 101, 143–157.

Rivas, I., Kumar, P., Hagen-Zanker, A., Andrade, M.F., Slovic, A.D., Pritchard, J.P., Geurs, K.T., 2017b. Determinants of black carbon, particle mass and number concentrations in London transport microenvironments. Atmos. Environ. 161, 247–262.

Salma, I., Weidinger, T., Maenhaut, W., 2007. Time-resolved mass concentration, composition and sources of aerosol particles in a metropolitan underground railway station. Atmos. Environ. 41, 8391–8405.

Sanders, P.G., Xu, N., Dalka, T.M., Maricq, M.M., 2003. Airborne brake wear debris: size distributions, composition, and a comparison of dynamometer and vehicle tests. Environ. Sci.Technol. 37, 4060–4069.

Saunders, B.M., Smith, J.D., Smith, T.E.L., Green, D.C., Barratt, B., 2019. Spatial variability of fine particulate matter pollution ($PM_{2.5}$) on the London underground network. Urban Clim. 30, 100535.

Seaton, A., Cherrie, J., Dennekamp, M., Donaldson, K., Hurley, J.F., Tran, C.L., 2005. The London underground: dust and hazards to health. Occup.Environ.Med. 62, 355.

Shen, H.Y., Anastasio, C., 2012. A comparison of hydroxyl radical and hydrogen peroxide generation in ambient particle extracts and laboratory metal solutions. Atmos. Environ. 46, 665–668.

Smith, J.D., Barratt, B.M., Fuller, G.W., Kelly, F.J., Loxham, M., Nicolosi, E., Priestman, M., Tremper, A.H., Green, D.C., 2020. $PM_{2.5}$ on the London underground. Environ. Int. 134, 105188.

STC, 2022. METRO: Línea 6. Available atSistema de Transporte Colectivo. https://www.metro.cdmx.gob.mx/la-red/linea-6. (Accessed 31 August 2022).

Sturm, R., 2016. Total deposition of ultrafine particles in the lungs of healthy men and women: experimental and theoretical results. Ann.Transl.Med. 4, 234.

Tan, S.T., Mohamed, N., Ng, L.C., Aik, J., 2022. Air quality in underground metro station commuter platforms in Singapore: a cross-sectional analysis of factors influencing commuter exposure levels. Atmos. Environ. 273, 118962.

TfL, 2020. https://tfl.gov.uk/corporate/about-tfl/what-we-do (accessed 30.05.2021).

TFL, 2020. Office of rail and road [WWW Document]. URLOff. Rail Regul (accessed 04.12.22) http://orr.gov.uk/statistics/published-stats/station-usage-estimates.

Theodorou, I.G., Ruenraroengsak, P., Gow, A., Schwander, S., Zhang, J., Chung, K.F., Tetley, T.D., Ryan, M.P., Porter, A.E., 2016. Effect of pulmonary surfactant on the dissolution, stability and uptake of zinc oxide nanowires by human respiratory epithelial cells. Nanotoxicology 10, 1351–1362.

Travar, I., Kihl, A., Kumpiene, J., 2015. The release of As, Cr and Cu from contaminated soil stabilized with APC residues under landfill conditions. J. Environ. Manag. 151, 1–10.

Tu, M., Olofsson, U., 2021. PM levels on an underground metro platform: a study of the train, passenger flow, urban background, ventilation, and night maintenance effects. Atmos. Environ:X 12, 100134.

Van Ryswyk, K.V., Anastasopolos, A.T., Evans, G., Sun, L., Sabaliauskas, K., Kulka, R., Wallace, L., Weichenthal, S., 2017. Metro commuter exposures to particulate air pollution and $PM_{2.5}$-associated elements in three Canadian cities: the urban transportation exposure study. Environ.Sci.Technol. 51, 5713–5720.

VentAxia, 2021. Ventilation Design Guidelines. https://www.vent-axia.com/. (Accessed 7 July 2020).

Vilcassim, M.J.R., Thurston, G.D., Peltier, R.E., Gordon, T., 2014. Black carbon and particulate matter ($PM_{2.5}$) concentrations in New York city's subway stations. Environ. Sci. Technol. 48, 14738–14745.

Wahlström, J., Söderberg, A., Olander, L., Jansson, A., Olofsson, U., 2010. A pin-on-disc simulation of airborne wear particles from disc brakes. Wear 268, 763–769.

Wang, X.R., Oliver Gao, H., 2011. Exposure to fine particle mass and number concentrations in urban transportation environments of New York City. Transp. Res. Part D: Transp. Environ. 16, 384–391.

WHO, 2021. WHO Global Air Quality Guidelines: Particulate Matter ($PM_{2.5}$ and PM_{10}), Ozone, Nitrogen Dioxide, Sulfur Dioxide and Carbon Monoxide. https://apps.who.int/iris/handle/10665/345329.

Xiao, Q.Y., Saikawa, E., Yokelson, R.J., Chen, P.F., Li, C.L., Kang, S.C., 2015. Indoor air pollution from burning yak dung as a household fuel in Tibet. Atmos. Environ. 102, 406–412.

Yan, C., Zheng, M., Yang, Q., Zhang, Q., Qiu, X., Zhang, Y., Fu, H., Li, X., Zhu, T., Zhu, Y., 2015. Commuter exposure to particulate matter and particle-bound PAHs in three transportation modes in Beijing, China. Environ. Pollut. 204, 199–206.

Yang, J., Chen, S., Quin, P., Lu, F., Liu, A., 2018. The effect of Subway expansions on vehicle congestion: evidence from Beijing. J. Environ. Econ. Manag. 88, 114–133.

Ye, X., Lian, Z., Jiang, C., Zhou, Z., Chen, H., 2010. Investigation of indoor environmental quality in Shanghai metro stations, China. Environ. Monit. Assess. 167, 643–651.